Morphology and sediment dynamics of Blossom Shoals at Icy Cape, Alaska

Emily Eidam[1], Jim Thomson[2], John Malito[3], and Lucia Hosekova[4]

[1]University of North Carolina at Chapel Hill
[2]University of Washington
[3]University of Texas at Austin
[4]University of Hawaii at Manoa

August 28, 2023

Abstract

Capes and cape-associated shoals represent sites of convergent sediment transport, and can provide points of relative coastal stability, navigation hazards, and offshore sand resources. Shoal evolution is commonly impacted by the regional wave climate. In the Arctic, changing sea-ice conditions are leading to (1) longer open-water seasons when waves can contribute to sediment transport, and (2) an intensified wave climate (related to duration of open water and expanding fetch). At Blossom Shoals offshore of Icy Cape in the Chukchi Sea, these changes have led to a five-fold increase in the amount of time that sand is mobile at a 31-m water depth site between the period 1953-1989 and the period 1990-2022. Wave conditions conducive to sand transport are still limited to less than 2% of the year, however - and thus it is not surprising that the overall morphology of the shoals has changed little in 70 years, despite evidence of active sand transport in the form of 1-m-scale sand waves on the flanks of the shoals which heal ice keel scours formed during the winter. Suspended-sediment transport is relatively weak due to limited sources of mud nearby, but can be observed in a net northeastward direction during the winter (driven by the Alaska Coastal Current under the ice) and in a southwestward direction during open-water wind events. Longer open-water seasons mean that annual net northeastward transport of fine sediment may weaken, with implications for the residence time of fine-grained sediments and particle-associated nutrients in the Chukchi Sea.

Eidam, E.F.[1,2], Thomson, J.[3], Malito, J.G.[2,4], Hošeková, L.[3,5]

Morphology and sediment dynamics of Blossom Shoals at Icy Cape, Alaska

[1]College of Earth, Ocean, and Atmospheric Sciences, Oregon State University, Corvallis, OR
[2]Department of Earth, Marine, and Environmental Sciences, University of North Carolina at Chapel Hill, Chapel Hill, USA
[3]Applied Physics Laboratory, University of Washington, Seattle, USA
[4]Texas Bureau of Economic Geology, Austin, TX
[5]University of Hawai'i at Mānoa, Honolulu, USA

Key Points:

- The bathymetry of Blossom Shoals has changed little between the 1950s and 2020, suggesting morphologic stability
- Duration of sand mobility due to waves has increased by ~7.5 days/year since the 1950s due to longer summer and larger waves
- Longer open-water seasons mean there is a potential for a reduction in annual net northeastward sediment transport

Corresponding author: Emily Eidam, `emily.eidam@oregonstate.edu`

Abstract

Capes and cape-associated shoals represent sites of convergent sediment transport, and can provide points of relative coastal stability, navigation hazards, and offshore sand resources. Shoal evolution is commonly impacted by the regional wave climate. In the Arctic, changing sea-ice conditions are leading to (1) longer open-water seasons when waves can contribute to sediment transport, and (2) an intensified wave climate (related to duration of open water and expanding fetch). At Blossom Shoals offshore of Icy Cape in the Chukchi Sea, these changes have led to a five-fold increase in the amount of time that sand is mobile at a 31-m water depth site between the period 1953-1989 and the period 1990-2022. Wave conditions conducive to sand transport are still limited to less than 2% of the year, however - and thus it is not surprising that the overall morphology of the shoals has changed little in 70 years, despite evidence of active sand transport in the form of 1-m-scale sand waves on the flanks of the shoals which heal ice keel scours formed during the winter. Suspended-sediment transport is relatively weak due to limited sources of mud nearby, but can be observed in a net northeastward direction during the winter (driven by the Alaska Coastal Current under the ice) and in a southwestward direction during open-water wind events. Longer open-water seasons mean that annual net northeastward transport of fine sediment may weaken, with implications for the residence time of fine-grained sediments and particle-associated nutrients in the Chukchi Sea.

Plain Language Summary

Offshore of coastal headlands, large sand ridges (on the scale of 1 m to 10 m high) commonly occur. These features can change shape and migrate over decades to centuries, especially conditions change in the ocean - for example, when wave energy increases and/or sea level rises. Here we explore the shape and sediments of Blossom Shoals offshore of Icy Cape in northwestern Alaska. These ridges are dominated by sands, though muds travel through the system during storms (and are likely sourced from the adjacent lagoons) and during the winter when sea ice covers the ocean. These shoals appear to have been changed little in shape over the past 70 years, though stronger waves in the present climate mean that sands in the shoals are mobile for more time each year, which means the shoals may change shape and/or location in the future. Muddy sediments tend to flow northeastward (on average) over the course of a year, but longer open-water seasons mean that these sediments may spend a greater portion of each year traveling southwestward - representing a possible change in the typical pathway of sediments and related nutrients (like carbon).

1 Introduction

Following the Last Glacial Maximum (18-20 kya), many coastal regions have experienced sea-level rise and coastal retreat, which in turn have provided a source of sand (i.e., from eroding shorelines) to the nearshore zone and continental shelves. Where hydrodynamic conditions and sediment supply have been suitable, these sediments have been sculpted by waves and currents into large sand banks, ridges, and bars on the inner to middle continental shelf (Dyer & Huntley, 1999). Cape-associated shoals are a subtype of these features which form offshore of coastal headlands (or points of relative coastal stability), as a result of convergent sediment transport driven by tidal currents and/or waves from alternating directions (Dyer & Huntley, 1999; McNinch & Luettich, 2000; Ashton et al., 2001). Cape-associated shoals commonly have relief on the order of of 1-10 m and cross-shore scales on the order of 1-10 km, and thus can pose navigation hazards and serve as potential sand resources (Tanner et al., 1963; Moslow & Heron, 1981; McNinch & Wells, 1999; Dyer & Huntley, 1999; Q. Wang et al., 2009; Pickens et al., 2021). These features can also contribute to the morphologic stability of adjacent headlands by dissipating wave energy, a process which in turn modulates longshore transport rates (e.g., McCarroll et al., 2020).

Some mid-latitude shoals have been thoroughly investigated in order to understand general coastal dynamics and manage risks and resources. Arctic shoals have received less attention (partly because of the logistical challenges of working in the Arctic during the brief open-water season), but their dynamics are integrated with overall coastal stability and relevant in light of increasing interests in Arctic development (shipping, port construction, etc.; Showstack, 2013) and changing environmental conditions (longer open-water seasons, Stroeve & Notz, 2018; more energetic wave climates, Thomson et al., 2016; and accelerating coastal retreat, Jones et al., 2009). Here we examine the morphology and sediment-transport dynamics of Blossom Shoals offshore of Icy Cape in northwest Alaska (Figure 1) to better understand how changing Arctic environmental conditions (e.g., intensifying wave climate) may impact shoals.

2 Background

2.1 Regional setting

Icy Cape is one of a series of cuspate headlands bordering the Chukchi Sea on the northwest Alaskan coastline (Figure 1). The Chukchi Sea is a shallow epicontinental sea (up to 50 m deep) which was inundated during sea-level rise following the Last Glacial Maximum. The shallow sea has accumulated ∼1–10 m of Holocene sediment cover on top of a reworked coastal plain (Creager & McManus, 1968; Grantz et al., 1982; Phillips et al., 1988). The islands flanking Icy Cape are part of the "longest, straightest, most stable, and best developed" barrier island chain in northern Alaska (Short, 1979). The region is impacted by dominantly southwesterly winds and waves, leading to northward longshore sediment transport – though Short (1979) notes that the north-facing capes (Cape Lisburne, Icy Cape, and Pt. Franklin) are dominated by onshore northeasterly winds. Regionally throughout northern Alaska (Cape Prince of Wales to the Canadian Border) coastal change rates have ranged from 20 m/yr of accretion to 16 m/yr of erosion between the 1950s and 2010s (Gibbs & Richmond, 2015; Gibbs et al., 2019). Within this region, however, Icy Cape has exhibited relatively modest coastal change rates since the 1950s, ranging from 4.3 m/yr (accretion) to –3.4 m/yr (erosion) (Gibbs et al., 2019). Spit and inlet morphology along Chukchi Sea coastlines indicate northward longshore transport (Short, 1979), but coastal change analyses for the 1950s versus 2010s suggest that the east side of Icy Cape is eroding while the west side is accreting (Gibbs et al., 2019; Figure 1C). The barrier islands on either side of the cape form shallow Kasegaluk Lagoon (Phillips & Reiss, 1984). The small Utukok River discharges ∼30 km south of the cape, and fine-grained sediments are thought to accumulate in the lagoon. The lagoon is connected to the inner continental shelf by shallow inlets (∼1.5 to 6 m deep; Phillips & Reiss, 1984), and is likely being infilled by flood-tide delta deposits related to inlet migration (Short, 1979).

In the nearshore zone around Icy Cape (<30 m depth), the Holocene sediment cover is generally ∼2 m thick, except in patchy locations where sediments are up to ∼8 m thick. Features such as infilled paleochannels and shoals occur sporadically and have sediment thicknesses of 15-23 m (Phillips & Reiss, 1984; Grantz et al., 1982). Low rates of accumulation are attributed to seabed erosion and low sediment supply. Some outcrops of

Cretaceous sedimentary bedrock occur throughout the region, including at ∼12 m water depth east of Icy Cape (Phillips & Reiss, 1984).

Immediately north of the cape, Blossom Shoals extend ∼20 km seaward with relief of 6–16 m, and represent a local sediment depocenter underalin by bedrock (Phillips & Reiss, 1984; Phillips et al., 1988). Shoal sediments are dominated by sands (with some gravels in the troughs), and adjacent beach sediments are very fine to fine gravel (Phillips & Reiss, 1984). Short (1975) reported the occurrence of submerged bars within 800 m of shore on both sides of the cape. Bars were oriented *en echelon* (oblique to shore) or parallel to shore depending on the wave approach angle.

The Chukchi Sea is typically ice-covered between mid-November and mid-June (Mahoney et al., 2014). Since the 1970s, the open-water season in this region has increased by ∼10 days per decade (Farquharson et al., 2018), allowing more time for wave energy to impact the coast annually. Increasing Arctic Ocean fetch has also led to a more energetic sea state in this region (Thomson & Rogers, 2014), an environmental shift which is expected to impact coastal erosion (Thomson et al., 2016). The effect of increased wave energy on sedimentary headland systems like Icy Cape and Blossom Shoals remains unknown.

Icy Cape lies roughly midway between the Bering Strait and Arctic Ocean. A 7-cm steric sea-surface height difference between the Pacific Ocean and Arctic Ocean drives northward baroclinic flow (Aagaard et al., 2006). Approximately 40% of this relatively warm inflow is contained in the Alaskan Coastal Current (ACC), which travels at speeds of 50-80 cm/s near Icy Cape (Barnes et al., 1983) and generates clockwise rotating eddies on the northern/eastern lee of each of the major regional headlands (Phillips et al., 1988). Flow within the ACC is modulated or reversed by northeasterly wind events occurring at intervals of days to weeks (Fang et al., 2017; Stabeno et al., 2018). Reversal of the typical northward flow requires a wind speed of 6 m/s sustained over several days (Fang et al., 2017), a condition which is exceeded for 5% of the open-water season. As a result, the surface current field offshore of Icy Cape tends to be bimodal in the alongshore direction (Fang et al., 2017, Stabeno et al., 2018, Woodgate & Aagaard, 2005, Woodgate et al., 2015).

Summertime eastern Chukchi Sea waters are typically well-stratified with cold, saline bottom water underlying warm, fresh meltwater (associated with sea ice) which hugs the coast (Stabeno et al., 2018, Woodgate et al., 2015). This two-layer stratification is homogenized during winter wind events (Woodgate & Aagaard, 2005, Woodgate et al., 2015). Seasonal variations lead to temperatures ranging from -2 to 2° C and salinities from 32 to 33 psu (Woodgate & Aagaard, 2005).

2.2 Morphologic similarities to temperate cape-associated shoals

Morphologically, the cape-shoal systems in the Chukchi Sea are not dissimilar from temperate systems such as the North Carolina capes. In both northwestern Alaska and North Carolina, capes are spaced every 100-150 km along the coast (Komar, 1976). The North Carolina capes likely evolved when sea levels stabilized ∼4000 years BP, and have been maintained by convergent longshore (wave-driven) sediment transport at the intersection of adjacent littoral cells (Moslow & Heron, 1981; McNinch & Luettich, 2000; Park & Wells, 2005; Thieler et al., 2014; Ashton et al., 2001). Residual tidal currents steered by the shoals are also thought to promote seaward sediment transport and shoal maintenance, even though the tidal range is microtidal (McNinch & Luettich, 2000). This type of convergent longshore transport and seaward sediment flux is likely active at Icy Cape as well, the the tidal range is also microtidal. In both the Arctic and temperate systems, smaller ripples and bedforms occur on top of shoal ridges, suggesting active modern seabed sediment transport (Phillips & Reiss, 1984; Hunt et al., 1977; Thieler et al., 2014).

2.3 Goals of this study

Here we (1) explore the modern morphology of Blossom Shoals and make comparisons to bathymetry from the 1950s, in order to assess apparent sediment-transport pathways and 70-year morphologic stability; (2) evaluate modern wave and current data and 70-year hindcast wave data, in order to assess how transport potential may be changing; and (3) evaluate local fine-sediment transport and bypassing associated with waves and coastal current interactions. Together these products provide a comprehensive modern and 70-year historic view of mud and sand dynamics associated with this shoal complex, which can serve as the foundation for future modeling efforts and aid in predictions of future cape evolution in a warming Arctic.

3 Methods

3.1 Data collection and processing

Bathymetric, sediment, and water-column data were collected from the *R/V Sikuliaq* in November 2019 (cruise SKQ201923S) and September/October 2020 (cruise SKQ202013S) as additions to the Coastal Ocean Dynamics in the Artic (CODA, www.apl.uw.edu/coda) project. Data were also collected from a small companion workboat in shallow water during the 2020 survey. Multibeam bathymetry data were collected from *R/V Sikuliaq* using a hull-mounted Kongsberg EM710 system (UAF, 2019). Data were gridded at 2-m resolution in MBSystem, open-source bathymetry processing software (`www.mbari.org/products/research-software/mb-system/`). Existing bathymetry from NOAA surveys H07753 (1950), H07665 (1950), and H08698 (1962) were downloaded from NCEI (`https://maps.ngdc.noaa.gov/viewers/bathymetry/`) and gridded at 50 m in MBSystem. Additional single-beam bathymetry data (and additional water-column profile data and grab samples - see below) were collected from a small companion workboat near shore during the 2020 survey. These data were not corrected for tides or motion correction, were smoothed for plotting, and are used only for qualitative comparisons of general shoal morphology and location.

Conductivity, temperature, depth, and turbidity profiles (CTDTu) were collected using an 8-Hz RBR Concerto profiling sensor. In situ volumetric particle-size distributions were measured using a Sequoia LISST200X laser diffraction sensor which was calibrated daily using DI water. LISST profiles were collected in triplicate at each station, and data from all three casts was aggregated, despiked, and averaged at one-meter depth intervals. Seabed grab samples were collected using a spring-loaded Shipek sampler or hand-operated mini Van Veen sampler. Samples were analyzed for grain-size distributions using an Escitec S3Plus laser diffraction sizer.

Between the 2019 and 2020 surveys, time-series data of water velocities and wave properties were collected at site S1A (at ∼30 m water depth) using a Nortek Signature 500 kHz upward-looking acoustic Doppler current profiler (ADCP) with wave mode mounted on a seabed tripod (Thomson et al., 2021; Hošeková et al., 2021; Figure 1). Wind data were downloaded from NOAA station WRXA2 (Wainwright, Alaska) which is located approximately 80 km northeast of Icy Cape (data were accessed from https://portal.aoos.org).

In 2019, intensive sampling was conducted during a wind event between 22 and 25 November. Grab samples and CTDTu/LISST profiles were collected repeatedly along transect S1 (Figure 1), as well as at a scattering of sites south of the transect, in conjunction with repeated SWIFT buoy deployments targeted at wave measurements (see Hošeková et al., 2020).

3.2 Modern and historical bed stresses and durations of critical stress exceedance

Shear stress acting on bed sediments (τ_b, $[N/m^2]$) is commonly quantified in marine environments for currents (τ_c), for waves (τ_w), or for combined wave-current effects (τ_{wc}). Within any of these three categories, the *critical* stress is defined as the bed shear stress needed to produce motion of sediment particles protruding from the seabed.

Shear stress due to unidirectional currents (τ_c) can be quantified using a quadratic stress law:

$$\tau_c = \rho C_D \bar{U}^2 \tag{1}$$

where ρ is the density of seawater (here assumed to be 1026 kg/m^3), C_D is a drag coefficient, and $\bar{U}$ is the free-stream flow speed outside of the bottom boundary layer. While the alternative logarithmic law of the wall (or Karman-Prandtl) equation is commonly used to derive shear stress or shear velocity, the quadratic stress law (Equation 1) better accounts for measurements made outside the near-bed logarithmic velocity layer from an upward-looking ADCP. Innumerable estimates and formulations for drag coefficients are available; here we choose a power law suitable for sands (Soulsby, 1997):

$$C_D = \alpha(\frac{z_0}{h})^\beta \tag{2}$$

where α is 0.0474, β is 1/3, z_0 is a roughness length, and h is the water depth. The roughness length can be calculated as $k_s/30$, where k_s is the Nikuradse roughness length (equal to 2.5$*d_{50}$, where d_{50} is the median - or 50th percentile - grain diameter). This formulation is applicable in the case of hydrodynamically rough flows (i.e., where the shear Reynolds number $u_* k_s/\nu$ is > 70; u_* is the bed shear velocity and ν is the kinematic viscosity). Because of the low current speeds and fine to medium sand substrate, flow in this system is in fact often not hydrodynamically rough, but Grant & Madsen (1979) note that in environments with waves, hydrodynmically rough flow is a reasonable approximation. The roughness length z_0 is thus estimated as 1.52e-5 m based on a measured d_{50} of 0.182 mm at S1A (see results in section 4). The mean water depth at S1A was 31.2 m.

The critical stress due to currents (τ_{cr}) is commonly expressed in terms of the Shields parameter (θ_c):

$$\theta_{cr} = \frac{\tau_{cr}}{g(\rho_s - \rho)d} \tag{3}$$

where g is the acceleration due to gravity, ρ_s is the density of sediment (assumed to be 2650 kg/m^3), ρ is the density of seawater (assumed to be 1026 kg/m^3), and d is the median grain size on the bed. This equation can be solved for τ_c after determining θ_{cr} from a Shields diagram (e.g., Soulsby & Whitehouse, 1997). This is problematic because the Shields diagram requires an iterative solution based on bed shear velocity (derived from shear stress). However, several empirically derived best-fit equations are available, including the following which allows for a non-iterative solution for τ_{cr} using seabed grain-size information (Soulsby & Whitehouse, 1997):

$$\theta_{cr} = \frac{0.30}{1 + 1.2D*} + 0.055[1 - exp(-0.020D*)] \tag{4}$$

where $D*$ is a dimensionless grain-size term equal to:

$$D* = [\frac{g((\rho_s/\rho) - 1)}{\nu^2}]^{1/3}d \tag{5}$$

In this equation, ν is the kinematic viscosity of seawater (assumed to be 1.818e-06 m^2/s), and d is assumed to be the median grain size of 0.182 mm sampled at S1A.

The shear stress due to waves is commonly calculated as:

$$\tau_w = \frac{1}{2}\rho f_w u_{bm}^2 \tag{6}$$

Where f_w (dimensionless) and u_{bm} ([m/s]) are the wave friction factor and maximum wave orbital velocity, respectively. Here we compute f_w following the method of Soulsby (1997):

$$f_w = 1.39 \frac{A}{z_0}^{-0.52} \tag{7}$$

where A is the semi-orbital excursion, equal to $u_b T/2\pi$ (u_b is the wave-orbital velocity in m/s and T is the wave period in s). The maximum wave-orbital velocity (u_{bm}) is commonly used here because it has the maximum impact on sediment transport. It depends on the wave height (H, [m]), wave period (T, [s]), water depth (h, [m]), and dimensionless wavenumber (k):

$$u_{bm} = \frac{\pi H}{T \sinh(kh)} \tag{8}$$

This term u_{bm} can be calculated using different summary statistics of wave height and wave period (e.g., significant wave height, mean wave height, peak wave period, mean wave period). Here we used H_{sig} and T_p (see discussion in Soulsby, 1987 and Wiberg & Sherwood, 2008) derived from up-looking Nortek ADCP data at the S1A site (see Thomson et al., 2021). The critical bed shear stress under waves can be computed by substituting τ_{wcr} and θ_{wcr} for τ_{cr} and θ_{cr}, respectively, in Equations 3 and 4 (see Soulsby & Whitehouse, 1997).

For combined waves and currents, the total measured shear stress (τ_{wc}) can be computed using parameters noted above and a wave-current interaction model (here we use the method in Madsen, 1994). The *critical* total or combined wave-current shear stress can be determined from the same equations used to determine critical current and critical wave stresses but with τ_{wcr} substituted for τ_{cr} (Equations 3 and 4; Soulsby & Whitehouse, 1997).

The above methods allow for calculation of total hours when the critical stress for local sediment is exceeded by currents, waves, and/or combined wave-current effects during some time period of observations. In this study, the total hours of stress exceedence by currents, waves, and combined wave-currents are computed for the period of mooring data (2019 to 2020). It is worth noting that for the free-stream velocity in Equation 1), we used the depth-averaged velocity between 3 and 21 m above the bed in order to suppress noise in the data. In order to assess historical changes in bed stresses, ERA5 climate hindcast wave data were also obtained (available through www.ecmwf.int) and used to determine the annual total hours of stress exceedance by waves.

4 Results

4.1 Seabed morphology and sediment textures

The bathymetry of the Blossom Shoals sand ridges in 2020 was relatively similar to the gridded bathymetry from the 1950s NOAA charts (Figure 2). The outer ridges had relief on the order of 7-15 m and wavelengths of 2400-3300 m both in the 1950s and in 2020. The inner ridges had relief of 3-7 m and wavelengths of 380-1000 m. Slopes of inner and outer ridges ranged from ~0.0044 to 0.028 m/m (or ~0.25° to 1.6°). The cross-sectional asymmetry of the outer ridges was variable, while inner ridges were slightly steeper on the seaward side. The inner ridges appeared to have migrated ~100-300 m seaward since the 1950s, but this apparent change may simply reflect interpolation error or geo-rectification error of sparse nearshore bathymetry in the older chart (e.g., Zimmerman et al., 2022).

Sand waves with heights on the order of 1 m and wavelengths on the order of 10 m were observed in patchy locations throughout the study area during both the 2019 and 2020 surveys (Figure 3). They appeared to generally occur on the flanks of the large sand ridges, and not in the troughs (consistent with observations by Phillips & Reiss, 1984). During the Nov 2019 survey (conducted during autumn storms), these sand waves appeared to be well-formed and intact, while during the Sep/Oct 2020 survey (i.e., earlier in the open water season prior to major storms), the bedforms exhibited some linear scarring consistent with other reports of ice keel scours (Figure 4; Phillips & Reiss, 1984).

Surficial seabed textures around Blossom Shoals were dominated by well-sorted, very fine to medium sands (d_{50} of 120-370 μm). Intermittent muds and gravels occurred in swales between ridges, and on the eastern side of the shoal complex (Figure 5). The coarsest sands were associated with the central axis of the shoals. Mud fractions were typically <20%, but ranged up to 55% in a few samples and were dominated by very fine silts. Gravel patches contained shell hash and were found inshore of the 10-m isobath.

4.2 Annual-scale sediment-transport pathways and forcing mechanisms

During the November 2019 to September 2020 mooring deployment at S1A (31-m depth), ice cover was present from mid-December to early May (Figure 6). Winds were variable but typically less than 10 m/s (Figure 6A). Water depths varied between ~30 and 32 m (Figure 6C), which primarily reflected wind dynamics (this area is microtidal). Currents at 3 meters above the bed were weakest during the ice-covered winter period, and strongest in November and December during the freezeup season. Current speeds were typically less than 0.3-0.5 m/s, except during brief events (Figure 6E). Current directions alternated between northeast and southwest (Figure 6C) and typically responded to changes in wind patterns (Figure 6B, D, F). Wave heights gradually increased throughout the open-water season from ∼0.5-1 m in the summer to ∼2-3 m in the fall (Figure 6G).

The long-term average current-driven bed stress (τ_c) was 0.075 N/m^2, less than the critical bed stress of 0.19 N/m^2 (Figure 6I). A few peaks in τ_c occurred throughout the deployment, leading to 786 hours of critical stress exceedance or "excess stress" by currents alone. This was equivalent to ∼10% of the November 2019 to September 2020 deployment period. The average wave-driven bed stress (τ_w) was 0.15 N/m^2. Multiple peaks in wave stress occurred, and the maximum value was 3.6 N/m^2. Wave stress exceeded the critical stress for 631 hours, or ∼8% of the deployment period. Waves contributed to excess stress primarily during September and November. Currents provided excess stress episodically throughout the entire deployment, including periods of ice cover (Figure 6K).

Near-bed suspended sediments (measured at 3 m above the bed) generally traveled parallel to the regional coastline (northeastward or southwestward; Figure 7A, C). During the fall storm season, transport was dominantly southwestward. During the winter-ice covered period, transport was dominantly northeastward. During the lower-energy summer open-water season, transport directions were variable over time scales corresponding to variations in wind patterns (figures 6C, 7A,). In surface waters, suspended-sediment transport was weaker and generally directed toward shore, except during fall freezeup and early winter when transport was directed dominantly along-coast (Figure 7).

4.3 Event-scale hydrodynamics and sediment transport

During the November 2019 wave event, CTDTu and LISST profiles were collected at the sites shown in Figure 8A at the same time that the mooring was deployed at S1A. Mooring time-series data from the event period are illustrated in Figure 8B-D, and size, turbidity, and temperature profiles from discrete locations in Figure 8A are presented in a stacked time-series view in Figure 8E-G. During the event, winds blew from the northeast for several days with variable speeds less than 5 m/s (Figures 6B, 8B). Toward the end of the event (Nov 23) onshore winds developed. Near-bed currents were generally southwestward (Figure 8C). Wave heights were generally >2 m with a peak on Nov 21 (Figures 6H, 8C). Wave-induced shear stresses exceeded the critical stress at that site for several days. In the water column, suspended-particle sizes were $\sim$100 μm during the peak in wave energy, but decreased throughout the rest of the period to <50 μm (Figure 8E). Turbidities were generally higher in shallower waters (up to $\sim$40 NTU) and near the bed at deeper sites (>40 NTU; Figure 8F). Warm water was mixed throughout the water column at some times early in the event, but by November 23 the inshore waters had cooled and offshore waters had re-stratified (Figure 8G). Water-column turbidities returned to near-background levels and suspended particle sizes decreased within a day of the change in wind and current direction and re-establishment of stratification.

4.4 Multidecadal trends in sediment transport potential

Based on the ERA5 trend analysis, the open-water season at Icy Cape has increased at a rate of $\sim$1.3 d/yr, similar to trends reported for the region by others (Farquharson et al., 2018; Figure 9A). It is worth noting that there was an apparent increase in the overall rate of change around 1990.

Also based on ERA5, the annual mean peak wave period increased at a rate of 0.019 s/yr (Figure 9B) and the annual mean significant wave height increased at a rate of 0.0050 m/yr (Figure 9C). These amount to increases of approximately 1 s in annual mean peak wave period and 0.35 m in significant wave height over the $\sim$70-year hindcast period. The annual mean shear stress, which ranged from $\sim$0.12 to 0.36 cm/s, also showed a slight increasing trend (Figure 9D).

The total hours of excess stress (or critical stress exceedance) generated by waves for sands increased at a rate of $\sim$2.6 hours per year ($\sim$7.6 days in 70 years; Figure 9E). Similar to the number of open-water days per year, this parameter appeared to increase more rapidly beginning in the 1990s. The mean value between 1953 and 1989 was 34 hrs per year, and the mean value between 1990 and 2022 was 148 hours per year - representing a roughly five-fold increase, but still a small fraction of the year (148 hours is 1.7% of the year). Based on a comparison of bed stress during the three years at the beginning of the record (1953-1955) versus the end of the record (2020-2022), the annual "stress climate" changed from a few brief storm peaks occurring during September/October to a prolonged period of storm peaks between September and mid-December (Figure 9). Bed stress also occurred earlier in the year at the end of the record, but values remained below the critical stress threshold until mid-September (similar to the beginning of the record).

5 Discussion

Icy Cape and Blossom Shoals represent a sandy cape-shoal system similar in morphology to some analogous temperate systems, but influenced by sea ice. Ice causes physical disturbance (keel scours), blocks wave energy in the winter, and alters current flow in the winter by sheltering the water water column from wind forces. The future evolution of Blossom Shoals under diminishing sea ice and increasing wave energy remains unknown. Here we summarize observed morphology and seasonal transport dynamics, and discuss the implications of the changing wave climate on sediment transport.

5.1 Morphology and sediment properties of Blossom Shoals and comparisons to two temperate shoals

The morphology of Blossom Shoals generally resembles that of other cape-associated shoals found in temperate latitudes. The largest sand ridges at Blossom Shoals are 3-15 m high with wavelengths of 400-3300 m and occur within ~2 km of shore. By comparison, Diamond Shoals offshore of Cape Hatteras are up to 10 m high, spaced up to 5000 m apart, and occur within 10 km of shore (Hunt et al., 1977). Cape Lookout Shoals are ~2-7 m high, spaced up to 2000 m apart, and occur within 16 km of shore (McNinch & Wells, 1999). All three of these example systems have formed inshore of the 30-m isobath in relatively low-relief microtidal shelf settings.

In Blossom Shoals, most sediments are very fine to coarse sand (0 to 4ϕ) with a relatively high degree of sorting (Figure 5), and the dominant size is fine sand (~2.3ϕ). Muds and gravels are found infrequently in troughs between sand ridges, and muds are most common northeast of the cape (Figure 5). Finding well-sorted sands is expected in this type of environment. Mud is relatively scarce - a few small rivers feed the Alaskan Chukchi margin, and as Phillips and Reiss (1984) suggest, the majority of the local fine-grained fluvial sediment load (silts and clays carried in suspension) is likely trapped in the adjacent lagoons (similar to the trapping that occurs in the lagoons backing the North Carolina capes). Fall storms, such as those observed in November 2019, likely generate waves and remobilization of some of this stored mud, which is then available to be advected through the inlets by currents (see also Phillips & Reiss, 1984). Outside of the lagoons, fine-grained sediment is transported past the shoals in low concentrations, but has little opportunity to deposit and accumulate except in a few sheltered areas between ridges during low-energy seasons. The several days of sustained excess wave stress during the November 2019 event highlight one of the barriers to deposition (Figures 6J, 8D).

The sands comprising Blossom Shoals are somewhat finer than the dominantly 0-2 ϕ sand found at Diamond Shoals in North Carolina (Hunt et al., 1977). The finer sizes in Blossom Shoals may reflect regional lithology of the source material, and/or possibly the reduced energy climate associated with up to 9 months of ice cover per year and limited fetch during the summer season.

In Blossom Shoals and the two North Carolina systems, small sand waves are superimposed on top of the sand ridges, and are interpreted as evidence of active bedload transport (Phillips & Reiss, 1984; Hunt et al., 1977; Thieler et al., 2014). In the case of Blossom Shoals, Phillips and Reiss (1984) noted that migration of these sand waves is also responsible for filling keel scours which form during the winter - a process which was observed in successive years in this study (Figure 4). Ice gouging thus does not seem to be a major agent of morphologic change, though it does cause local and temporary disturbance.

Because there are so many morphologic similarities between Blossom Shoals and some North Carolina systems, it is interesting that the two temperate systems extend farther from shore than the arctic system (10-16 km in North Carolina, versus 2 km for Blossom Shoals). This raises the question of whether Blossom Shoals is limited in extent because there is too little sediment in the longshore transport cells to feed it, and/or because convergent offshore transport is too limited by the brief open-water season (and/or weak wave climate) to promote more extensive seaward shoal growth. In either case, a longer open-water season combined with a related intensification in wave climate could promote stronger longshore transport (which would accelerate sediment delivery to the headland) and consequently stronger offshore transport through convergence of longshore sediment flux from east and west. Transport patterns would also depend, of course, on sediment supplies and on the nature of the convergent currents, mediated by winds, waves, and the Alaska Coastal Current.

Over the past 70 years, the morphology of Blossom Shoals has been relatively stable in profile view (Figure 2). The large, concentric sand ridges appear to have migrated little, if at all, since the 1950s NOAA surveys (Figure 2), and the smaller bedforms found on the sides of the large sand ridges are remarkably similar in terms of locations and geometry to those described by Phillips and Reiss (1984). It thus appears that the shoal system has existed in a state of dynamic equilibrium not yet perturbed by changes in wave climate and a lengthening open-water season. An exception may be the small sand ridges most proximal to the headland, which appear to have migrated slightly seaward on the order of 100 m laterally - but due to the sparse data interpolated from the older survey charts, these changes should not be over-interpreted. These inner shoals may also behave somewhat differently than the outer shoals because of the dynamics of landfast ice. In the Arctic, landfast ice tends to form earlier in the fall than offshore ice, and break up later in the spring - and at this site, landfast ice tends to form inshore of site S1A (see Hošeková et al., 2020 and Hošeková et al., 2021 for discussions of landfast ice at this site).

5.2 Suspended-sediment transport dynamics

While fine-grained sediments (silts and clays) are found only in sheltered patches within the shoals, their transport during an annual cycle lends insight into general sediment pathways and potential bypassing around the shoals (with potential implications for nutrient transport and substrate character).

During the winter after ice forms, a weak signal of fine-grained suspended-sediment transport is observed near-bed with a persistent northeastward direction (Figure 7A). This wintertime suspended sediment follows the pathway of the Alaska Coastal current. During the open-water season, episodic wind events like those illustrated in Figure 6 (right column) and Figure 8 (first part of time series) disrupt this current flow. During these types of events, waves drive resuspension and elevated water-column turbidities, particularly in shallow nearshore zones (where mud tends to be more available; Figures 5, 8F). Wind-driven currents mix the water column (Figure 8E, F, G), disrupt the northeastward flow of the Alaska Coastal Current (Figure 8B, C), and drive brief southwestward transport of suspended sediments near bed (and landward transport of sediments near the surface; Figure 7). Annually, however, the net transport direction appears to be northeastward, meaning there should be a net transfer of particles toward the Arctic Ocean (and perhaps Barrow Canyon farther north). Given a longer open-water season, this net northeastward transport may weaken. This could have several implications include reduced northeastward transport of any sediment-associated nutrients and longer residence time of fine-grained sediments within the Chukchi Sea.

5.3 Measured and projected bed stresses

Seabed stresses imposed by waves and currents (and combined wave-current effects) are commonly used in sediment transport-rate equations. It is thus useful to evaluate seasonal variability in bed stresses to determine when the sands comprising the shoals are most likely to be mobile (i.e., times of excess stress, as noted in section 5.2), as well as interannual variability in mobility, in order to better predict whether sand transport potential has changed over the past few decades and determine the direction of present trends.

Between the early 1950s and mid-1990s, the mean number of open-water days per year was typically 50-150 at site S1A (which is outside the modern seasonal landfast ice zone observed by Hošeková et al., 2021). Excess stress generated by waves occurred for a much smaller portion of the year (<100 hrs per year; Figure 9A, E). This excess stress typically only occurred toward the end of the open-water season, in September. In the mid-1990s, the length of the open-water season began increasing to typical values closer to 200 days per year. This change was logically accompanied by an intensification of the wave climate (see Figure 9B, C), which has been attributed to increasing fetch as a consequence of increasing seasonal retreat of pack ice in the Arctic Ocean (Thomson & Rogers, 2014; Khon et al., 2014; X. L. Wang et al., 2015; Thomson et al., 2016; Liu et al., 2016; Casas-Prat et al., 2018). The increasing number of open-water days and more energetic sea states have jointly created a longer season of more frequent critical stress exceedence (Figure 9F). Interestingly, this period of high bed stress doesn't appear to start earlier than it did in the 1950s, which is likely a consequence of the onset of the fall storm season set by processes in the northern Pacific. But this high-stress period does extend much later into the year - i.e., into mid-December rather than mid-October. Consequently, the number of hours of sand mobility per year have increased.

It is worth noting that these changes may be conservative estimates of how the stress distribution has changed for the shoals, because (1) they don't account for currents and (2) these data are from a relatively deep site (S1A, 31 m). The actual bed stress acting on the seafloor is a non-linear combination of wave and current stress. Currents are not represented in the multidecadal analysis (Figure 9) because of limitations in the hindcast data, and currents would serve to amplify the stress imposed by waves. In terms of water depth, S1A is likely below the wave base for many locally and distally generated waves. Multidecadal reductions in sea ice have allowed for larger, longer-period waves to develop, which should provide increasing bed stress at site S1A and on the outer shoals. The inner shoals are likely impacted in a different way. While these longer-period waves may attenuate before they reach the inner shoals, the longer open-water season means there is a longer period each year when smaller waves can impact the shoals - though the multidecadal trends in landfast ice (which buffer the inner shoals against wave energy) are not well-known.

The increasingly long exposure to excess stress (at least at the outer shoals) should create greater rates of bedload transport in the shoals. Thus far, the shoals do not appear to have migrated substantially in response to these changes, unless the morphologic differences within 3 km of shore can be interpreted as meaningful (Figure 2; see also section 4.1). However, at some point in the future they will likely reach a tipping point when the overall morphology may change. A morphodynamic model of shoal evolution would be helpful in predicting such changes. Challenges to modeling would include (1) assessing the source term of sediment, i.e., rates of longshore drift and sizes of material supplied from adjacent shorelines and (2) assessing how eddies shed by the Alaska Coastal Current around the headland may influence the net directions of sediment transport (given that the Alaska Coastal Current is not necessarily static in time).

6 Conclusions

Icy Cape and Blossom Shoals are a cape-shoal system located along the Chukchi Sea coast in northwestern Alaska which represent a site of convergent sediment transport similar in nature to analogous temperate systems, such as the the multiple cuspate headlands forming the Outer Banks in North Carolina. Blossom Shoals consists of large sand ridges with relief of several meters and spacing of hundreds of meters. Patches of sand waves with relief on the order of a meter and spacing of tens of meters occur on the flanks of the larger ridges in many locations, and indicate active several transport (as evidenced by the "healing" of ice keel scours between seasons).

Unlike temperate systems, much of the wave-enhanced sediment transport that occurs is limited to the brief open-water season (though currents do act throughout the year - including during the winter - to occasionally mobilize seabed sands). The influence of waves is increasing due to increasingly energetic sea states and increasingly long periods of open water, which are both a consequence of diminishing Arctic pack ice. Based on modeled wave hindcasts for the past $\sim$70 years, the typical number of hours of excess stress generated by waves (at a $\sim$30-m site) has increased from $<$ 100 hours per year to $\sim$100-200 hours per year. Recent measurements suggest that annual hours of stress exceedence may be much higher. To date the shoals have exhibited little morphologic change, but a morphodynamic model which accounts for changes in seastate would be a worthwhile next step to assess whether a tipping point in morphology evolution may occur given further increases in wave exposure. The role and future fate of landfast ice, which historically occurs within 10 km of the shore, should also be considered since it may dramatically affect the total wave exposure in the inshore portion of the shoal (Hošeková et al., 2021).

Fine-grained sediments are sparse, but their transport is regulated by wind events and winter ice conditions. During the winter, suspended sediment travels in a net northeastward direction, toward the Arctic Basin. During wind events in the open-water season, this direction is reversed - though the net transport direction is still dominated by winter conditions. If the length of the open-water season maintains its present trajectory, there is a potential for the net transport direction to change, which could have implications for residence time of fine-grained sediment in the Chukchi Sea and nutrient pathways.

Acknowledgments

This work was funded by NSF OPP 1913195 and OPP 1818485. We thank the captains and crew of *R/V Sikuliaq* and Alex de Klerk for assistance in data collection, and

Steve Roberts for assistance with 1950s bathymetry acquisition and gridding, as well as McKenzie McLean, Owen White, and Tyler Souza for assistance with sample processing and discussions of results.

The S1A mooring data are available at http://hdl.handle.net/1773/47139 or

https://doi.org/10.18739/A2DF6K45W. The grain-size and water-column profile data are available at the Arctic Data Center under doi:10.18739/A2862BD1G (Eidam et al., 2023).

References

Aagaard, K., Weingartner, T. J., Danielson, S. L., Woodgate, R. A., Johnson, G. C., & Whitledge, T. E. (2006). Some controls on flow and salinity in Bering Strait. *Geophysical Research Letters*, *33*(19).

Ashton, A., Murray, A. B., & Arnoult, O. (2001). Formation of coastline features by large-scale instabilities induced by high-angle waves. *Nature*, *414*(6861), 296–300.

Barnes, P. W., Reimnitz, E., Hunter, R. E., Phillips, R. L., & Wolf, S. (1983). Geologic processes and hazards of the Beaufort and Chukchi Sea shelf and coastal regions. *OCSEAP Final Report, Research Unit*, *205*, 1–18.

Casas-Prat, M., Wang, X. L., & Swart, N. (2018). CMIP5-based global wave climate projections including the entire arctic ocean. *Ocean Modelling*, *123*, 66–85.

Creager, J. S., & McManus, D. A. (1968). *Geology of the floor of Bering and Chukchi Seas: American studies.* University of Washington Department of Oceanography.

Dyer, K. R., & Huntley, D. A. (1999). The origin, classification and modelling of sand banks and ridges. *Continental Shelf Research*, *19*(10), 1285–1330.

Eidam, E., Thomson, J., Malito, J., & Hošeková, L. (2023). *Blossom Shoals water-column, seabed sediment, and bathymetry data. Icy Cape, Chukchi Sea, Alaska. 2019-2020.* Arctic Data Center. Retrieved from `https://arcticdata.io/catalog/view/doi:10.18739/A2862BD1G`

Fang, Y., Potter, R. A., Statscewich, H., Weingartner, T. J., Winsor, P., & Irving, B. K. (2017, December). Surface Current Patterns in the Northeastern Chukchi Sea and Their Response to Wind Forcing. *Journal of Geophysical Research: Oceans*, *122*(12), 9530–9547. Retrieved 2021-01-26, from https://onlinelibrary.wiley.com/doi/abs/10.1002/2017JC013121 doi: 10.1002/2017JC013121

Farquharson, L. M., Mann, D., Swanson, D., Jones, B., Buzard, R., & Jordan, J. (2018). Temporal and spatial variability in coastline response to declining sea-ice in northwest Alaska. *Marine Geology*, *404*, 71–83.

Gibbs, A. E., Nolan, M., Richmond, B. M., Snyder, A. G., & Erikson, L. H. (2019). Assessing patterns of annual change to permafrost bluffs along the North Slope coast of Alaska using high-resolution imagery and elevation models. *Geomorphology*, *336*, 152–164.

Gibbs, A. E., & Richmond, B. M. (2015). *National assessment of shoreline change: historical shoreline change along the north coast of Alaska, US-Canadian border to Icy Cape.* US Department of the Interior, US Geological Survey Reston, VA, USA.

Grant, W. D., & Madsen, O. S. (1979). Combined wave and current interaction with a rough bottom. *Journal of Geophysical Research: Oceans*, *84*(C4), 1797–1808.

Grantz, A., Dinter, D. A., Hill, E., May, S., McMullin, R., Phillips, R., & Reimnitz, E. (1982). *Geologic framework, hydrocarbon potential, and environmental conditions for exploration and development of proposed oil and gas lease sale 87 in the Beaufort and northeast Chukchi Seas: A summary report* (Tech. Rep.). US Geological Survey.

Hošeková, L., Eidam, E., Panteleev, G., Rainville, L., Rogers, W. E., & Thomson, J. (2021). Landfast ice and coastal wave exposure in northern Alaska. *Geophysical Research Letters*, *48*(22), e2021GL095103.

Hošeková, L., Malila, M. P., Rogers, W. E., Roach, L. A., Eidam, E., Rainville, L., … Thomson, J. (2020). Attenuation of ocean surface waves in pancake and frazil sea ice along the coast of the Chukchi Sea. *Journal of Geophysical Research: Oceans*, *125*(12), e2020JC016746.

Hunt, R. E., Swift, D. J., & Palmer, H. (1977). Constructional shelf topography, Diamond Shoals, North Carolina. *Geological Society of America Bulletin*, *88*(2), 299–311.

Jones, B. M., Arp, C. D., Jorgenson, M. T., Hinkel, K. M., Schmutz, J. A., & Flint, P. L. (2009). Increase in the rate and uniformity of coastline erosion in Arctic Alaska. *Geophysical Research Letters*, *36*(3), n/a–n/a. Retrieved from http://dx.doi.org/10.1029/2008GL036205 (L03503) doi: 10.1029/2008GL036205

Khon, V., Mokhov, I., Pogarskiy, F., Babanin, A., Dethloff, K., Rinke, A., & Matthes, H. (2014). Wave heights in the 21st century Arctic Ocean simulated with a regional climate model. *Geophysical Research Letters*, *41*(8), 2956–2961.

Komar, P. (1976). *Beach processes and sedimentation.* Prentice-Hall, Inc., New Jersey.

Liu, Q., Babanin, A. V., Zieger, S., Young, I. R., & Guan, C. (2016). Wind and wave climate in the Arctic Ocean as observed by altimeters. *Journal of Climate*, *29*(22), 7957–7975.

Madsen, O. S. (1994). Spectral wave-current bottom boundary layer flows. In *Coastal Engineering 1994* (pp. 384–398).

Mahoney, A. R., Eicken, H., Gaylord, A. G., & Gens, R. (2014). Landfast sea ice extent in the Chukchi and Beaufort Seas: The annual cycle and decadal variability. *Cold Regions Science and Technology*, *103*, 41–56.

McCarroll, R. J., Masselink, G., Valiente, N. G., Wiggins, M., Scott, T., Conley, D. C., & King, E. V. (2020, April). Impact of a headland-associated sandbank on shoreline dynamics. *Geomorphology*, *355*, 107065. Retrieved 2021-01-26, from https://linkinghub.elsevier.com/retrieve/pii/S0169555X20300374 doi: 10.1016/j.geomorph.2020.107065

McNinch, J. E., & Luettich, R. A. (2000). Physical processes around a cuspate foreland: implications to the evolution and long-term maintenance of a cape-associated shoal. *Continental Shelf Research*, 23.

McNinch, J. E., & Wells, J. T. (1999, June). Sedimentary processes and depositional history of a cape-associated shoal, Cape Lookout, North Carolina. *Marine Geology*, *158*(1-4), 233–252. Retrieved 2021-01-26, from https://linkinghub.elsevier.com/retrieve/pii/S0025322798001698 doi: 10.1016/S0025-3227(98)00169-8

Moslow, T. F., & Heron, S. D. J. (1981). Holocene depositional history of a microtidal cuspate foreland cape: Cape Lookout, North Carolina. *Marine Geology*, *41*(3-4), 251–270.

Park, J.-Y., & Wells, J. T. (2005). Longshore transport at Cape Lookout, North Carolina: shoal evolution and the regional sediment budget. *Journal of coastal re-*

search, *21*(1), 1–17.

Phillips, R., Barnes, P., Hunter, R., Reiss, T., & Rearic, D. (1988). *Geologic investigations in the Chukchi Sea, 1984, NOAA ship SURVEYOR cruise* (Tech. Rep.). US Geological Survey,.

Phillips, R., & Reiss, T. (1984). *Nearshore marine geologic investigations, Icy Cape to Wainwright, northeast Chukchi Sea.* US Department of the Interior, Geological Survey.

Pickens, B. A., Taylor, J. C., Finkbeiner, M., Hansen, D., & Turner, L. (2021). Modeling sand shoals on the US Atlantic shelf: Moving beyond a site-by-site approach. *Journal of Coastal Research*, *37*(2), 227–237.

Short, A. D. (1975, March). Offshore Bars along the Alaskan Arctic Coast. *The Journal of Geology*, *83*(2), 209–221. Retrieved 2021-01-26, from `https://www.journals.uchicago.edu/doi/10.1086/628082` doi: 10.1086/628082

Short, A.-D. (1979). Barrier island development along the Alaskan-Yukon coastal plains. *Geological Society of America Bulletin*, *90*(1_Part_II), 77–103.

Showstack, R. (2013). Diminishing Sea Ice in the Arctic Presents Challenges and Opportunities. *Eos Trans. AGU*, *94*(31), 270–271. doi: 10.1002/2013EO310002

Soulsby, R. (1987). Calculating bottom orbital velocity beneath waves. *Coastal Engineering*, *11*(4), 371–380.

Soulsby, R. (1997). *Dynamics of marine sands.* Howbery Park, London, 142 pp.: HR Wallingford.

Soulsby, R., & Whitehouse, R. (1997). Threshold of sediment motion in coastal environments. *Pacific Coasts and Ports' 97: Proceedings of the 13th Australasian Coastal and Ocean Engineering Conference and the 6th Australasian Port and Harbour Conference; Volume 1*, 145–150.

Stabeno, P., Kachel, N., Ladd, C., & Woodgate, R. (2018). Flow patterns in the eastern Chukchi Sea: 2010–2015. *Journal of Geophysical Research: Oceans*, *123*(2), 1177–1195.

Stroeve, J., & Notz, D. (2018, sep). Changing state of Arctic sea ice across all seasons. *Environmental Research Letters*, *13*(10), 103001. Retrieved from `https://doi.org/10.1088%2F1748-9326%2Faade56` doi: 10.1088/1748-9326/aade56

Tanner, W., Evans, R., & Holmes, C. (1963). Low-energy coast near cape romano, florida. *Journal of Sedimentary Research*, *33*(3), 713–722.

Thieler, E. R., Foster, D. S., Himmelstoss, E. A., & Mallinson, D. J. (2014). Geologic framework of the northern North Carolina, USA inner continental shelf and its influence on coastal evolution. *Marine Geology*, *348*, 113–130.

Thomson, J., Eidam, E., & Hošeková, L. (2021). *Mooring results from Coastal Ocean Dynamics in the Arctic (CODA).* University of Washington. Retrieved from https://digital.lib.washington.edu/researchworks/handle/1773/47139

Thomson, J., Fan, Y., Stammerjohn, S., Stopa, J., Rogers, W. E., Girard-Ardhuin, F., ... others (2016). Emerging trends in the sea state of the Beaufort and Chukchi seas. *Ocean Modelling*, *105*, 1–12.

Thomson, J., & Rogers, W. E. (2014). Swell and sea in the emerging Arctic Ocean. *Geophysical Research Letters*, *41*(9), 3136–3140.

UAF. (2019). *Rolling Deck to Repository, Sikuliaq* (Tech. Rep. No. SKQ201923S). University of Alaska Fairbanks. (DOI : 10.7284/908599 (accessed December 21, 2022).)

Wang, Q., Zhang, M., Zhong, S., Du, G., Jin, B., Yang, H., & Song, C. (2009, September). Dynamic sedimentation and geomorphologic evolution of the Laizhou shoal, Bohai sea, Northern China. *Journal of Asian Earth Sciences*, *36*(2-3), 196–208. Retrieved 2021-01-26, from https://linkinghub.elsevier.com/retrieve/pii/S1367912009001333 doi: 10.1016/j.jseaes.2009.06.001

Wang, X. L., Feng, Y., Swail, V. R., & Cox, A. (2015). Historical changes in the beaufort-chukchi-bering seas surface winds and waves, 1971-2013. *Journal of Climate*, *28*(19), 7457–7469.

Wiberg, P. L., & Sherwood, C. R. (2008). Calculating wave-generated bottom orbital velocities from surface-wave parameters. *Computers & Geosciences*, *34*(10), 1243–1262.

Woodgate, R. A., & Aagaard, K. (2005). Revising the Bering Strait freshwater flux into the Arctic Ocean. *Geophysical Research Letters*, *32*(2).

Woodgate, R. A., Stafford, K. M., & Prahl, F. G. (2015). A synthesis of year-round interdisciplinary mooring measurements in the Bering Strait (1990–2014) and the RUSALCA years (2004–2011). *Oceanography*, *28*(3), 46–67.

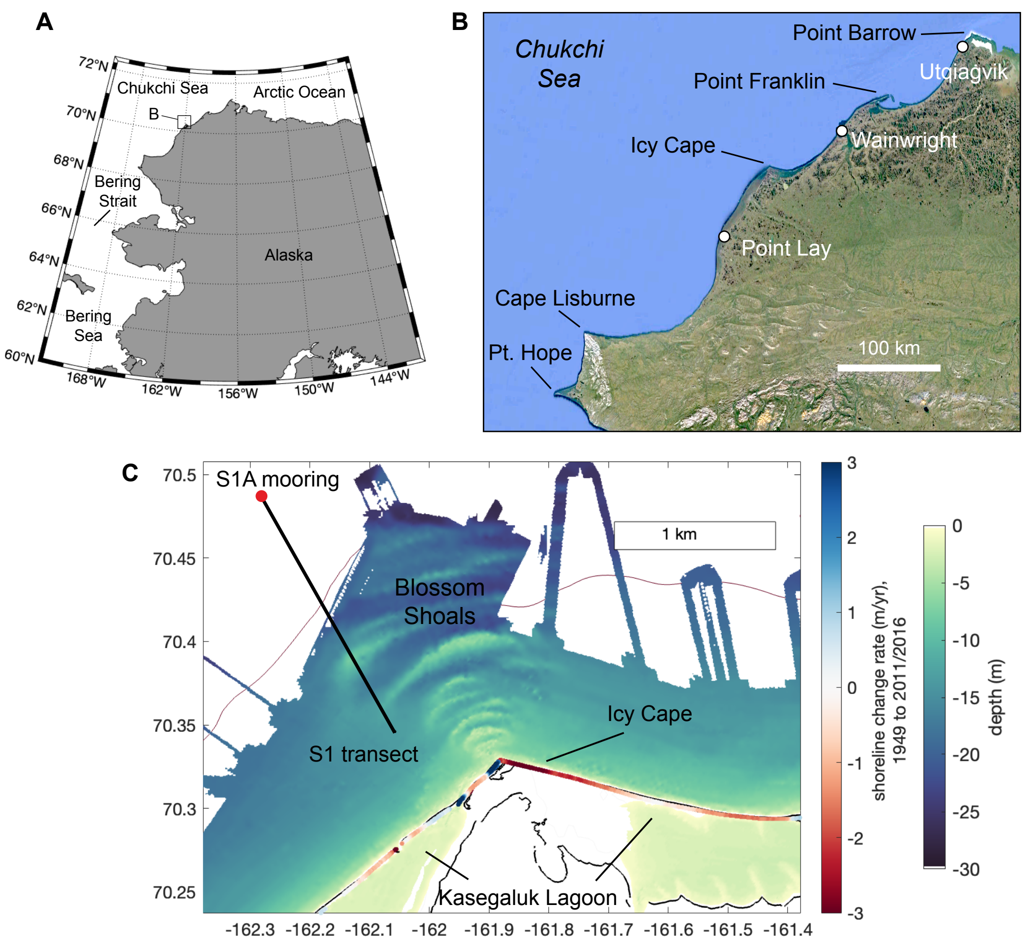

Figure 1: Vicinity maps. A) Icy Cape is located in northwestern Alaska on the Chukchi Sea. B) Cuspate headlands of northwestern Alaska, including Icy Cape. C) Blossom Shoals extend seaward a few kilometers from Icy Cape. Sources of bathymetry and shoreline change data provided in text.

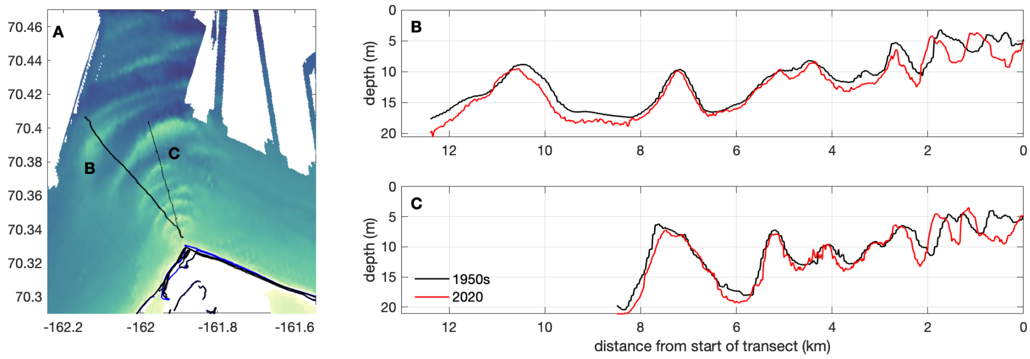

Figure 2: Shoal bathymetry. a) Gridded 1950s bathymetry of Blossom Shoals. b) Southern elevation profile of the shoals, from 1950 (based on gridded NOAA charts; see text) and 2020 (using a single-beam system on a small boat). c) Same as (b) for northern transect shown in (a). Vertical errors are not well-constrained and not shown. The general location of shoals which are >2 km from shore has remained relatively unchanged in 70 years (see discussion in text.

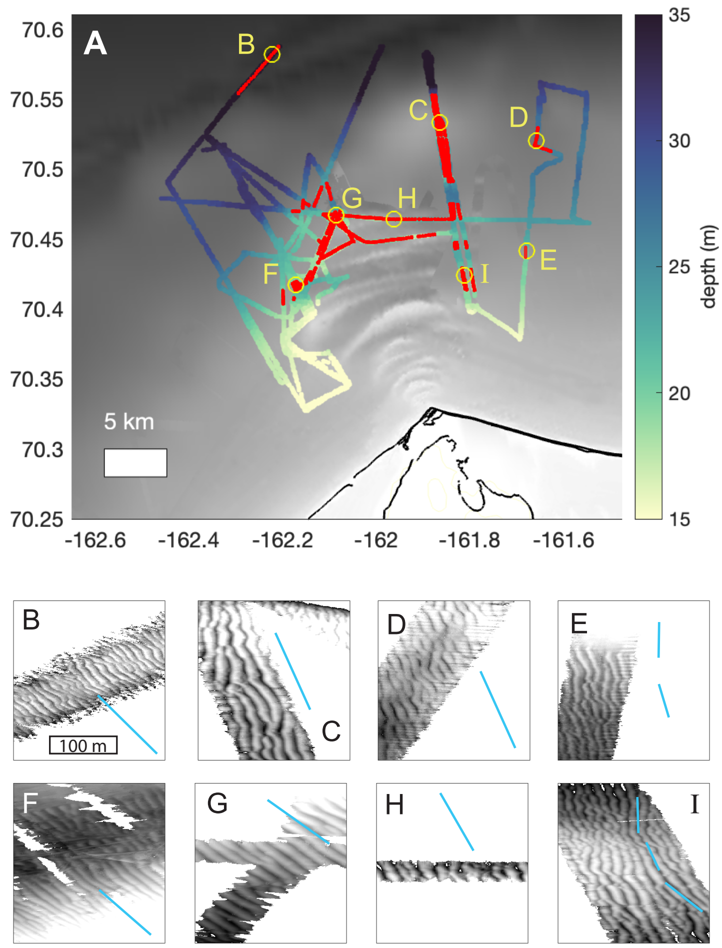

Figure 3: Bedform occurrence and details. A) Bedform occurrence (red) along 2019 and 2020 survey tracks (shaded by depth). Yellow dots denote regions highlighted in subsequent panels. (B-F) Details of ripples. Scale in each panel is the same. Blue lines denote general orientation of bedform crests. Bedform heights were typically 1 m and wavelengths were on the order of 10-20 m.

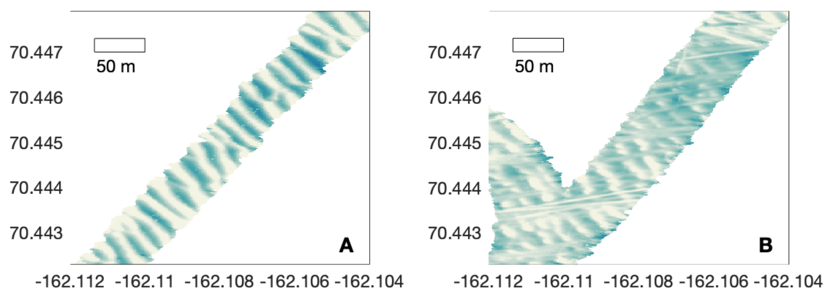

Figure 4: Detail of the change in bedforms between (A) November 2019 and (B) October 2020 at the same location (near site G in Figure 3. Note the linear scarring in (B); these data were collected earlier in the season than those in panel (A)

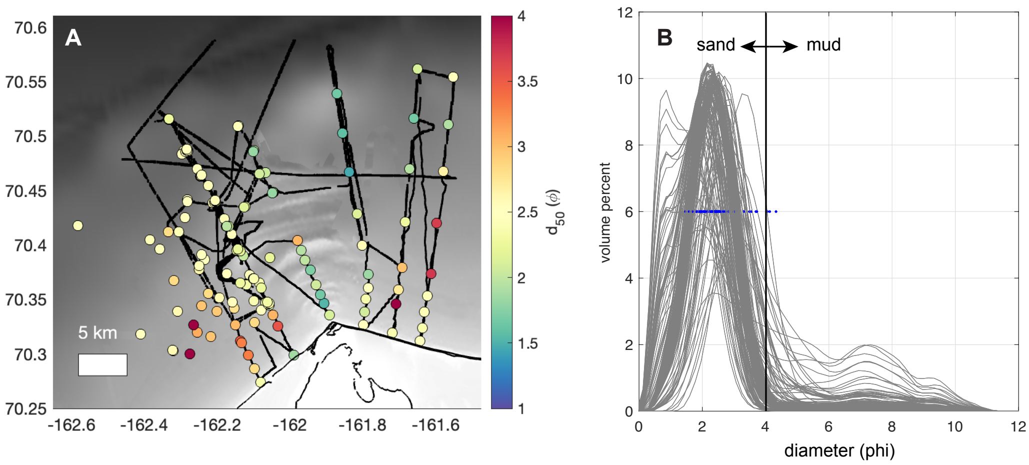

Figure 5: Seabed grain sizes. A) Map of median sediment diameter (d_{50}) reported on the phi scale (the $\log_2$ of the diameter in millimeters). Ship survey tracks are shown in black. Sediments were generally sandy except for a few regions near shore where muds were dominant. B) Aggregated histograms (by volume percent) for sample sites shown in (A). Blue dots denote d_{50} values. Histograms are shown to provide context regarding sorting (i.e., the width of the grain-size distribution peaks). Sand sizes from 1 to 3 phi were common (coarse to fine sand). Note that bimodal samples represent mud-dominated sites. FIX HISTOGRAM TO INCLUDE 2020 DATA

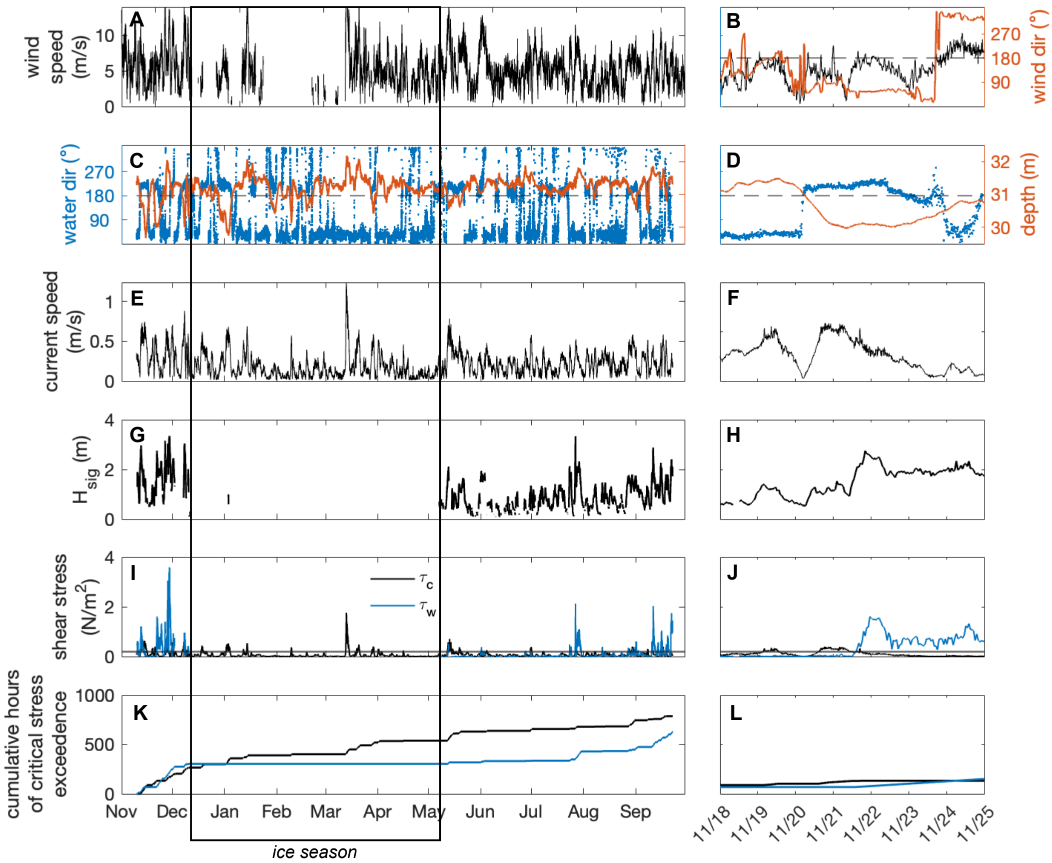

Figure 6: Meteorological data (from Wainwright) and mooring data (from S1A) for 2019 to 2020. The panels at left span the entire mooring record and the panels at right show a magnified view of mid-November 2019, when high-density vessel-based sampling was conducted. A, B) Wind speed. C, D) Water direction and depth. E, F) Current speed averaged between 3 and 21 meters above the bed. G, H) Significant wave height. I, J) Current and wave shear stress (with critical stress shown by the horizontal line). K, L) Cumulative hours when the critical stress was exceeded by waves or currents.

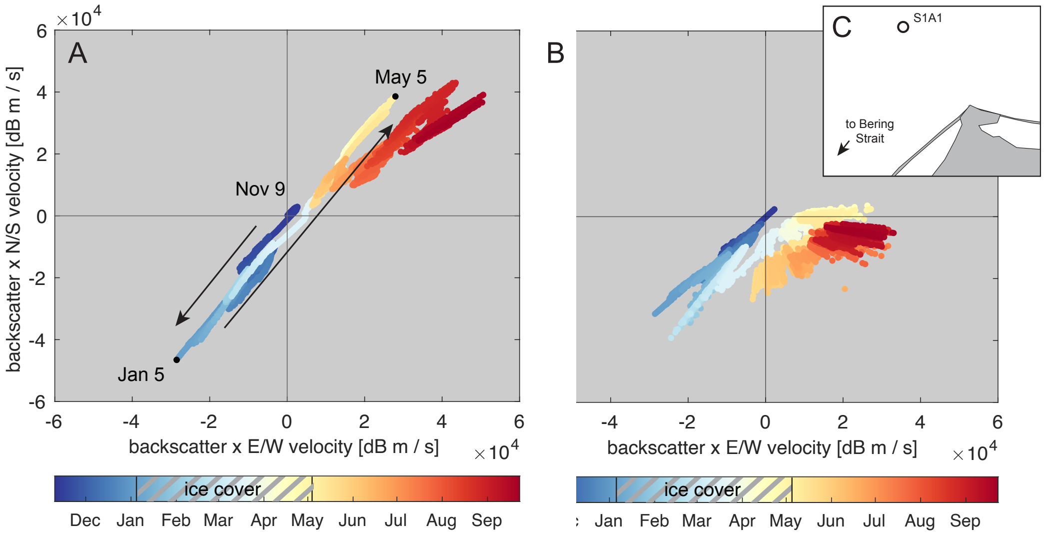

Figure 7: Cumulative sediment flux (proxy measure, using ADCP backscatter multiplied by velocity) in earth coordinates for the mooring deployment period, at site S1A. A) Flux at 3 meters above the bed. Arrows denote major net transport directions in fall (left) and winter (right). Ice cover was present from early January to May 5. Jan 5 and May 5 denote the transition points when the general flux direction abruptly changed. B) Flux at 21 meters above the bed (near the water surface). C) Schematic of local shoreline orientation for reference.

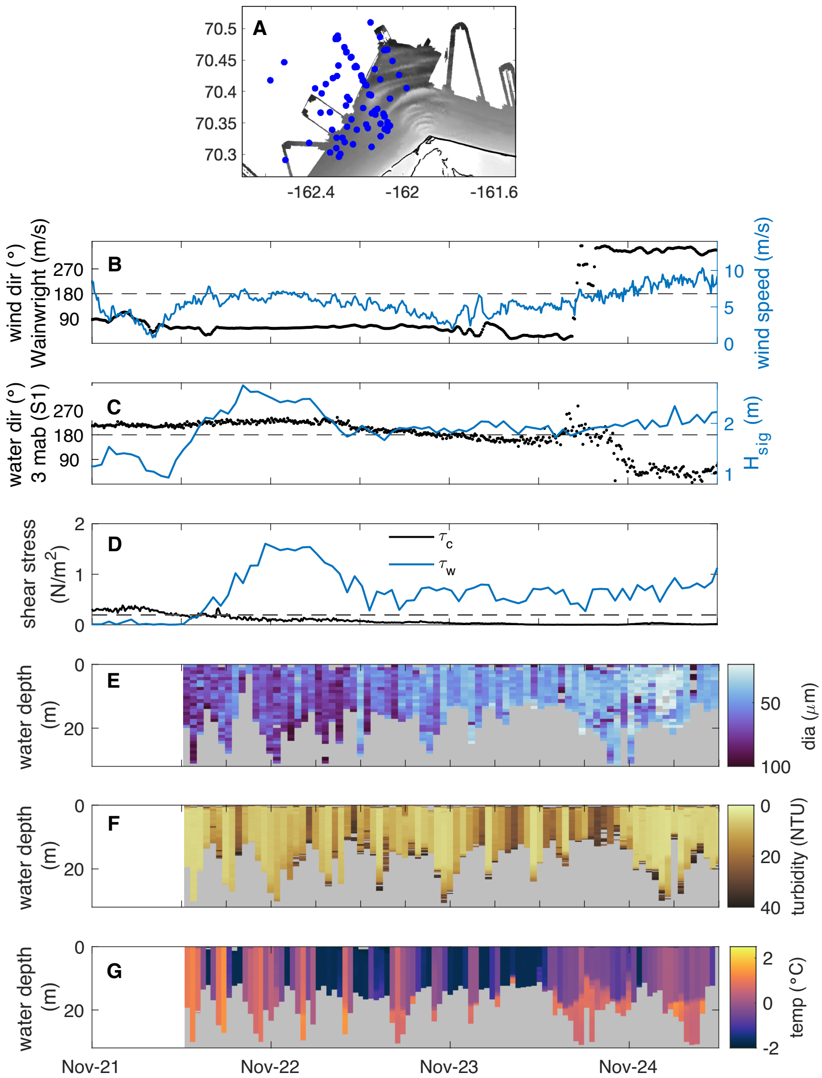

Figure 8: Hydrodynamics and water-column properties during the November 2019 wave event. A) Locations of CTDTu/LISST profiles. B) Wind direction and wind speed at Wainwright (see Figure 1B). C) Water direction and significant wave height at the S1A tripod (31 m water depth, 3 m above bed). D) Bed shear stress at S1A (current- and wave-induced). E) Water-column profiles of mean particle diameter throughout the study area. F) Water-column profiles of turbidity. G) Water-column profiles of temperature. Note that panels E-G are presented as time series though each profile was collected at a different location (the sites in A). They are shown in this fashion to give a general sense of the temporal evolution of suspended-sediment characteristics.

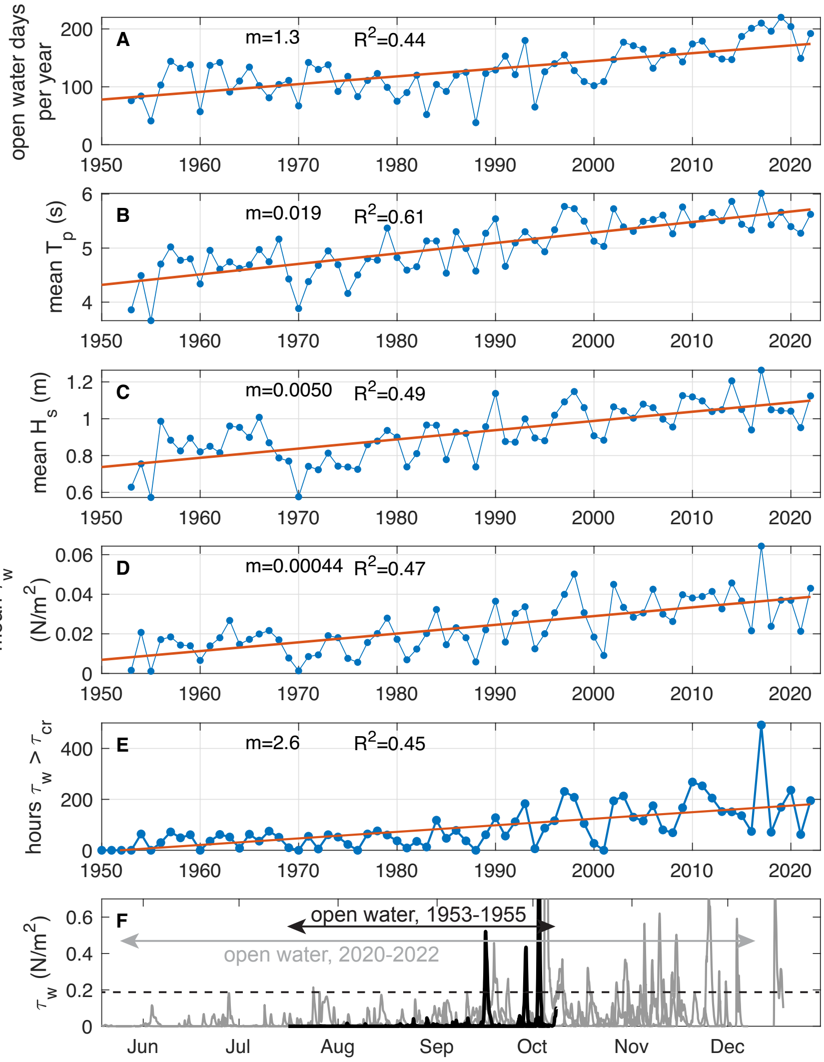

Figure 9: Multi-decadal trends in parameters related to waves and bed stresses, derived from ERA5 output. A) Number of open-water days per year. B) Mean peak wave period during each annual open-water season. C) Mean significant wave height during each annual open-water season. D) Mean τ_w during each annual open-water season (calculated from T_p and H_s). E) Cumulative number of hours per year when $\tau_w > \tau_{wcr}$ (0.196 N/m^2). F) Seasonal record of τ_w calculated from ERA5 output for the years 1954-1956 (black) and 2020-2022 (gray). The dashed line denotes τ_{wcr}.

Eidam, E.F.[1,2], Thomson, J.[3], Malito, J.G.[2,4], Hošeková, L.[3,5]

Morphology and sediment dynamics of Blossom Shoals at Icy Cape, Alaska

[1]College of Earth, Ocean, and Atmospheric Sciences, Oregon State University, Corvallis, OR
[2]Department of Earth, Marine, and Environmental Sciences, University of North Carolina at Chapel Hill, Chapel Hill, USA
[3]Applied Physics Laboratory, University of Washington, Seattle, USA
[4]Texas Bureau of Economic Geology, Austin, TX
[5]University of Hawai'i at Mānoa, Honolulu, USA

Key Points:

- The bathymetry of Blossom Shoals has changed little between the 1950s and 2020, suggesting morphologic stability
- Duration of sand mobility due to waves has increased by ~7.5 days/year since the 1950s due to longer summer and larger waves
- Longer open-water seasons mean there is a potential for a reduction in annual net northeastward sediment transport

Corresponding author: Emily Eidam, `emily.eidam@oregonstate.edu`

Abstract

Capes and cape-associated shoals represent sites of convergent sediment transport, and can provide points of relative coastal stability, navigation hazards, and offshore sand resources. Shoal evolution is commonly impacted by the regional wave climate. In the Arctic, changing sea-ice conditions are leading to (1) longer open-water seasons when waves can contribute to sediment transport, and (2) an intensified wave climate (related to duration of open water and expanding fetch). At Blossom Shoals offshore of Icy Cape in the Chukchi Sea, these changes have led to a five-fold increase in the amount of time that sand is mobile at a 31-m water depth site between the period 1953-1989 and the period 1990-2022. Wave conditions conducive to sand transport are still limited to less than 2% of the year, however - and thus it is not surprising that the overall morphology of the shoals has changed little in 70 years, despite evidence of active sand transport in the form of 1-m-scale sand waves on the flanks of the shoals which heal ice keel scours formed during the winter. Suspended-sediment transport is relatively weak due to limited sources of mud nearby, but can be observed in a net northeastward direction during the winter (driven by the Alaska Coastal Current under the ice) and in a southwestward direction during open-water wind events. Longer open-water seasons mean that annual net northeastward transport of fine sediment may weaken, with implications for the residence time of fine-grained sediments and particle-associated nutrients in the Chukchi Sea.

Plain Language Summary

Offshore of coastal headlands, large sand ridges (on the scale of 1 m to 10 m high) commonly occur. These features can change shape and migrate over decades to centuries, especially conditions change in the ocean - for example, when wave energy increases and/or sea level rises. Here we explore the shape and sediments of Blossom Shoals offshore of Icy Cape in northwestern Alaska. These ridges are dominated by sands, though muds travel through the system during storms (and are likely sourced from the adjacent lagoons) and during the winter when sea ice covers the ocean. These shoals appear to have been changed little in shape over the past 70 years, though stronger waves in the present climate mean that sands in the shoals are mobile for more time each year, which means the shoals may change shape and/or location in the future. Muddy sediments tend to flow northeastward (on average) over the course of a year, but longer open-water seasons mean that these sediments may spend a greater portion of each year traveling southwestward - representing a possible change in the typical pathway of sediments and related nutrients (like carbon).

1 Introduction

Following the Last Glacial Maximum (18-20 kya), many coastal regions have experienced sea-level rise and coastal retreat, which in turn have provided a source of sand (i.e., from eroding shorelines) to the nearshore zone and continental shelves. Where hydrodynamic conditions and sediment supply have been suitable, these sediments have been sculpted by waves and currents into large sand banks, ridges, and bars on the inner to middle continental shelf (Dyer & Huntley, 1999). Cape-associated shoals are a subtype of these features which form offshore of coastal headlands (or points of relative coastal stability), as a result of convergent sediment transport driven by tidal currents and/or waves from alternating directions (Dyer & Huntley, 1999; McNinch & Luettich, 2000; Ashton et al., 2001). Cape-associated shoals commonly have relief on the order of of 1-10 m and cross-shore scales on the order of 1-10 km, and thus can pose navigation hazards and serve as potential sand resources (Tanner et al., 1963; Moslow & Heron, 1981; McNinch & Wells, 1999; Dyer & Huntley, 1999; Q. Wang et al., 2009; Pickens et al., 2021). These features can also contribute to the morphologic stability of adjacent headlands by dissipating wave energy, a process which in turn modulates longshore transport rates (e.g., McCarroll et al., 2020).

Some mid-latitude shoals have been thoroughly investigated in order to understand general coastal dynamics and manage risks and resources. Arctic shoals have received less attention (partly because of the logistical challenges of working in the Arctic during the brief open-water season), but their dynamics are integrated with overall coastal stability and relevant in light of increasing interests in Arctic development (shipping, port construction, etc.; Showstack, 2013) and changing environmental conditions (longer open-water seasons, Stroeve & Notz, 2018; more energetic wave climates, Thomson et al., 2016; and accelerating coastal retreat, Jones et al., 2009). Here we examine the morphology and sediment-transport dynamics of Blossom Shoals offshore of Icy Cape in northwest Alaska (Figure 1) to better understand how changing Arctic environmental conditions (e.g., intensifying wave climate) may impact shoals.

2 Background

2.1 Regional setting

Icy Cape is one of a series of cuspate headlands bordering the Chukchi Sea on the northwest Alaskan coastline (Figure 1). The Chukchi Sea is a shallow epicontinental sea (up to 50 m deep) which was inundated during sea-level rise following the Last Glacial Maximum. The shallow sea has accumulated ∼1–10 m of Holocene sediment cover on top of a reworked coastal plain (Creager & McManus, 1968; Grantz et al., 1982; Phillips et al., 1988). The islands flanking Icy Cape are part of the "longest, straightest, most stable, and best developed" barrier island chain in northern Alaska (Short, 1979). The region is impacted by dominantly southwesterly winds and waves, leading to northward longshore sediment transport – though Short (1979) notes that the north-facing capes (Cape Lisburne, Icy Cape, and Pt. Franklin) are dominated by onshore northeasterly winds. Regionally throughout northern Alaska (Cape Prince of Wales to the Canadian Border) coastal change rates have ranged from 20 m/yr of accretion to 16 m/yr of erosion between the 1950s and 2010s (Gibbs & Richmond, 2015; Gibbs et al., 2019). Within this region, however, Icy Cape has exhibited relatively modest coastal change rates since the 1950s, ranging from 4.3 m/yr (accretion) to –3.4 m/yr (erosion) (Gibbs et al., 2019). Spit and inlet morphology along Chukchi Sea coastlines indicate northward longshore transport (Short, 1979), but coastal change analyses for the 1950s versus 2010s suggest that the east side of Icy Cape is eroding while the west side is accreting (Gibbs et al., 2019; Figure 1C). The barrier islands on either side of the cape form shallow Kasegaluk Lagoon (Phillips & Reiss, 1984). The small Utukok River discharges ∼30 km south of the cape, and fine-grained sediments are thought to accumulate in the lagoon. The lagoon is connected to the inner continental shelf by shallow inlets (∼1.5 to 6 m deep; Phillips & Reiss, 1984), and is likely being infilled by flood-tide delta deposits related to inlet migration (Short, 1979).

In the nearshore zone around Icy Cape (<30 m depth), the Holocene sediment cover is generally ∼2 m thick, except in patchy locations where sediments are up to ∼8 m thick. Features such as infilled paleochannels and shoals occur sporadically and have sediment thicknesses of 15-23 m (Phillips & Reiss, 1984; Grantz et al., 1982). Low rates of accumulation are attributed to seabed erosion and low sediment supply. Some outcrops of

Cretaceous sedimentary bedrock occur throughout the region, including at ∼12 m water depth east of Icy Cape (Phillips & Reiss, 1984).

Immediately north of the cape, Blossom Shoals extend ∼20 km seaward with relief of 6–16 m, and represent a local sediment depocenter underalin by bedrock (Phillips & Reiss, 1984; Phillips et al., 1988). Shoal sediments are dominated by sands (with some gravels in the troughs), and adjacent beach sediments are very fine to fine gravel (Phillips & Reiss, 1984). Short (1975) reported the occurrence of submerged bars within 800 m of shore on both sides of the cape. Bars were oriented *en echelon* (oblique to shore) or parallel to shore depending on the wave approach angle.

The Chukchi Sea is typically ice-covered between mid-November and mid-June (Mahoney et al., 2014). Since the 1970s, the open-water season in this region has increased by ∼10 days per decade (Farquharson et al., 2018), allowing more time for wave energy to impact the coast annually. Increasing Arctic Ocean fetch has also led to a more energetic sea state in this region (Thomson & Rogers, 2014), an environmental shift which is expected to impact coastal erosion (Thomson et al., 2016). The effect of increased wave energy on sedimentary headland systems like Icy Cape and Blossom Shoals remains unknown.

Icy Cape lies roughly midway between the Bering Strait and Arctic Ocean. A 7-cm steric sea-surface height difference between the Pacific Ocean and Arctic Ocean drives northward baroclinic flow (Aagaard et al., 2006). Approximately 40% of this relatively warm inflow is contained in the Alaskan Coastal Current (ACC), which travels at speeds of 50-80 cm/s near Icy Cape (Barnes et al., 1983) and generates clockwise rotating eddies on the northern/eastern lee of each of the major regional headlands (Phillips et al., 1988). Flow within the ACC is modulated or reversed by northeasterly wind events occurring at intervals of days to weeks (Fang et al., 2017; Stabeno et al., 2018). Reversal of the typical northward flow requires a wind speed of 6 m/s sustained over several days (Fang et al., 2017), a condition which is exceeded for 5% of the open-water season. As a result, the surface current field offshore of Icy Cape tends to be bimodal in the alongshore direction (Fang et al., 2017, Stabeno et al., 2018, Woodgate & Aagaard, 2005, Woodgate et al., 2015).

Summertime eastern Chukchi Sea waters are typically well-stratified with cold, saline bottom water underlying warm, fresh meltwater (associated with sea ice) which hugs the coast (Stabeno et al., 2018, Woodgate et al., 2015). This two-layer stratification is homogenized during winter wind events (Woodgate & Aagaard, 2005, Woodgate et al., 2015). Seasonal variations lead to temperatures ranging from -2 to 2° C and salinities from 32 to 33 psu (Woodgate & Aagaard, 2005).

2.2 Morphologic similarities to temperate cape-associated shoals

Morphologically, the cape-shoal systems in the Chukchi Sea are not dissimilar from temperate systems such as the North Carolina capes. In both northwestern Alaska and North Carolina, capes are spaced every 100-150 km along the coast (Komar, 1976). The North Carolina capes likely evolved when sea levels stabilized ∼4000 years BP, and have been maintained by convergent longshore (wave-driven) sediment transport at the intersection of adjacent littoral cells (Moslow & Heron, 1981; McNinch & Luettich, 2000; Park & Wells, 2005; Thieler et al., 2014; Ashton et al., 2001). Residual tidal currents steered by the shoals are also thought to promote seaward sediment transport and shoal maintenance, even though the tidal range is microtidal (McNinch & Luettich, 2000). This type of convergent longshore transport and seaward sediment flux is likely active at Icy Cape as well, the the tidal range is also microtidal. In both the Arctic and temperate systems, smaller ripples and bedforms occur on top of shoal ridges, suggesting active modern seabed sediment transport (Phillips & Reiss, 1984; Hunt et al., 1977; Thieler et al., 2014).

2.3 Goals of this study

Here we (1) explore the modern morphology of Blossom Shoals and make comparisons to bathymetry from the 1950s, in order to assess apparent sediment-transport pathways and 70-year morphologic stability; (2) evaluate modern wave and current data and 70-year hindcast wave data, in order to assess how transport potential may be changing; and (3) evaluate local fine-sediment transport and bypassing associated with waves and coastal current interactions. Together these products provide a comprehensive modern and 70-year historic view of mud and sand dynamics associated with this shoal complex, which can serve as the foundation for future modeling efforts and aid in predictions of future cape evolution in a warming Arctic.

3 Methods

3.1 Data collection and processing

Bathymetric, sediment, and water-column data were collected from the *R/V Sikuliaq* in November 2019 (cruise SKQ201923S) and September/October 2020 (cruise SKQ202013S) as additions to the Coastal Ocean Dynamics in the Artic (CODA, www.apl.uw.edu/coda) project. Data were also collected from a small companion workboat in shallow water during the 2020 survey. Multibeam bathymetry data were collected from *R/V Sikuliaq* using a hull-mounted Kongsberg EM710 system (UAF, 2019). Data were gridded at 2-m resolution in MBSystem, open-source bathymetry processing software (`www.mbari.org/products/research-software/mb-system/`). Existing bathymetry from NOAA surveys H07753 (1950), H07665 (1950), and H08698 (1962) were downloaded from NCEI (`https://maps.ngdc.noaa.gov/viewers/bathymetry/`) and gridded at 50 m in MBSystem. Additional single-beam bathymetry data (and additional water-column profile data and grab samples - see below) were collected from a small companion workboat near shore during the 2020 survey. These data were not corrected for tides or motion correction, were smoothed for plotting, and are used only for qualitative comparisons of general shoal morphology and location.

Conductivity, temperature, depth, and turbidity profiles (CTDTu) were collected using an 8-Hz RBR Concerto profiling sensor. In situ volumetric particle-size distributions were measured using a Sequoia LISST200X laser diffraction sensor which was calibrated daily using DI water. LISST profiles were collected in triplicate at each station, and data from all three casts was aggregated, despiked, and averaged at one-meter depth intervals. Seabed grab samples were collected using a spring-loaded Shipek sampler or hand-operated mini Van Veen sampler. Samples were analyzed for grain-size distributions using an Escitec S3Plus laser diffraction sizer.

Between the 2019 and 2020 surveys, time-series data of water velocities and wave properties were collected at site S1A (at ∼30 m water depth) using a Nortek Signature 500 kHz upward-looking acoustic Doppler current profiler (ADCP) with wave mode mounted on a seabed tripod (Thomson et al., 2021; Hošeková et al., 2021; Figure 1). Wind data were downloaded from NOAA station WRXA2 (Wainwright, Alaska) which is located approximately 80 km northeast of Icy Cape (data were accessed from https://portal.aoos.org).

In 2019, intensive sampling was conducted during a wind event between 22 and 25 November. Grab samples and CTDTu/LISST profiles were collected repeatedly along transect S1 (Figure 1), as well as at a scattering of sites south of the transect, in conjunction with repeated SWIFT buoy deployments targeted at wave measurements (see Hošeková et al., 2020).

3.2 Modern and historical bed stresses and durations of critical stress exceedance

Shear stress acting on bed sediments (τ_b, $[N/m^2]$) is commonly quantified in marine environments for currents (τ_c), for waves (τ_w), or for combined wave-current effects (τ_{wc}). Within any of these three categories, the *critical* stress is defined as the bed shear stress needed to produce motion of sediment particles protruding from the seabed.

Shear stress due to unidirectional currents (τ_c) can be quantified using a quadratic stress law:

$$\tau_c = \rho C_D \bar{U}^2 \tag{1}$$

where ρ is the density of seawater (here assumed to be 1026 kg/m^3), C_D is a drag coefficient, and $\bar{U}$ is the free-stream flow speed outside of the bottom boundary layer. While the alternative logarithmic law of the wall (or Karman-Prandtl) equation is commonly used to derive shear stress or shear velocity, the quadratic stress law (Equation 1) better accounts for measurements made outside the near-bed logarithmic velocity layer from an upward-looking ADCP. Innumerable estimates and formulations for drag coefficients are available; here we choose a power law suitable for sands (Soulsby, 1997):

$$C_D = \alpha(\frac{z_0}{h})^{\beta} \tag{2}$$

where α is 0.0474, β is 1/3, z_0 is a roughness length, and h is the water depth. The roughness length can be calculated as $k_s/30$, where k_s is the Nikuradse roughness length (equal to 2.5$*d_{50}$, where d_{50} is the median - or 50th percentile - grain diameter). This formulation is applicable in the case of hydrodynamically rough flows (i.e., where the shear Reynolds number $u_* k_s/\nu$ is > 70; u_* is the bed shear velocity and ν is the kinematic viscosity). Because of the low current speeds and fine to medium sand substrate, flow in this system is in fact often not hydrodynamically rough, but Grant & Madsen (1979) note that in environments with waves, hydrodynmically rough flow is a reasonable approximation. The roughness length z_0 is thus estimated as 1.52e-5 m based on a measured d_{50} of 0.182 mm at S1A (see results in section 4). The mean water depth at S1A was 31.2 m.

The critical stress due to currents (τ_{cr}) is commonly expressed in terms of the Shields parameter (θ_c):

$$\theta_{cr} = \frac{\tau_{cr}}{g(\rho_s - \rho)d} \tag{3}$$

where g is the acceleration due to gravity, ρ_s is the density of sediment (assumed to be 2650 kg/m^3), ρ is the density of seawater (assumed to be 1026 kg/m^3), and d is the median grain size on the bed. This equation can be solved for τ_c after determining θ_{cr} from a Shields diagram (e.g., Soulsby & Whitehouse, 1997). This is problematic because the Shields diagram requires an iterative solution based on bed shear velocity (derived from shear stress). However, several empirically derived best-fit equations are available, including the following which allows for a non-iterative solution for τ_{cr} using seabed grain-size information (Soulsby & Whitehouse, 1997):

$$\theta_{cr} = \frac{0.30}{1 + 1.2D*} + 0.055[1 - exp(-0.020D*)] \tag{4}$$

where $D*$ is a dimensionless grain-size term equal to:

$$D* = [\frac{g((\rho_s/\rho) - 1)}{\nu^2}]^{1/3} d \tag{5}$$

In this equation, ν is the kinematic viscosity of seawater (assumed to be 1.818e-06 m^2/s), and d is assumed to be the median grain size of 0.182 mm sampled at S1A.

The shear stress due to waves is commonly calculated as:

$$\tau_w = \frac{1}{2}\rho f_w u_{bm}^2 \tag{6}$$

Where f_w (dimensionless) and u_{bm} ([m/s]) are the wave friction factor and maximum wave orbital velocity, respectively. Here we compute f_w following the method of Soulsby (1997):

$$f_w = 1.39 \frac{A}{z_0}^{-0.52} \tag{7}$$

where A is the semi-orbital excursion, equal to $u_b T/2\pi$ (u_b is the wave-orbital velocity in m/s and T is the wave period in s). The maximum wave-orbital velocity (u_{bm}) is commonly used here because it has the maximum impact on sediment transport. It depends on the wave height (H, [m]), wave period (T, [s]), water depth (h, [m]), and dimensionless wavenumber (k):

$$u_{bm} = \frac{\pi H}{T \sinh(kh)} \tag{8}$$

This term u_{bm} can be calculated using different summary statistics of wave height and wave period (e.g., significant wave height, mean wave height, peak wave period, mean wave period). Here we used H_{sig} and T_p (see discussion in Soulsby, 1987 and Wiberg & Sherwood, 2008) derived from up-looking Nortek ADCP data at the S1A site (see Thomson et al., 2021). The critical bed shear stress under waves can be computed by substituting τ_{wcr} and θ_{wcr} for τ_{cr} and θ_{cr}, respectively, in Equations 3 and 4 (see Soulsby & Whitehouse, 1997).

For combined waves and currents, the total measured shear stress (τ_{wc}) can be computed using parameters noted above and a wave-current interaction model (here we use the method in Madsen, 1994). The *critical* total or combined wave-current shear stress can be determined from the same equations used to determine critical current and critical wave stresses but with τ_{wcr} substituted for τ_{cr} (Equations 3 and 4; Soulsby & Whitehouse, 1997).

The above methods allow for calculation of total hours when the critical stress for local sediment is exceeded by currents, waves, and/or combined wave-current effects during some time period of observations. In this study, the total hours of stress exceedence by currents, waves, and combined wave-currents are computed for the period of mooring data (2019 to 2020). It is worth noting that for the free-stream velocity in Equation 1), we used the depth-averaged velocity between 3 and 21 m above the bed in order to suppress noise in the data. In order to assess historical changes in bed stresses, ERA5 climate hindcast wave data were also obtained (available through www.ecmwf.int) and used to determine the annual total hours of stress exceedance by waves.

4 Results

4.1 Seabed morphology and sediment textures

The bathymetry of the Blossom Shoals sand ridges in 2020 was relatively similar to the gridded bathymetry from the 1950s NOAA charts (Figure 2). The outer ridges had relief on the order of 7-15 m and wavelengths of 2400-3300 m both in the 1950s and in 2020. The inner ridges had relief of 3-7 m and wavelengths of 380-1000 m. Slopes of inner and outer ridges ranged from $\sim$0.0044 to 0.028 m/m (or $\sim 0.25°$ to $1.6°$). The cross-sectional asymmetry of the outer ridges was variable, while inner ridges were slightly steeper on the seaward side. The inner ridges appeared to have migrated $\sim$100-300 m seaward since the 1950s, but this apparent change may simply reflect interpolation error or geo-rectification error of sparse nearshore bathymetry in the older chart (e.g., Zimmerman et al., 2022).

Sand waves with heights on the order of 1 m and wavelengths on the order of 10 m were observed in patchy locations throughout the study area during both the 2019 and 2020 surveys (Figure 3). They appeared to generally occur on the flanks of the large sand ridges, and not in the troughs (consistent with observations by Phillips & Reiss, 1984). During the Nov 2019 survey (conducted during autumn storms), these sand waves appeared to be well-formed and intact, while during the Sep/Oct 2020 survey (i.e., earlier in the open water season prior to major storms), the bedforms exhibited some linear scarring consistent with other reports of ice keel scours (Figure 4; Phillips & Reiss, 1984).

Surficial seabed textures around Blossom Shoals were dominated by well-sorted, very fine to medium sands (d_{50} of 120-370 μm). Intermittent muds and gravels occurred in swales between ridges, and on the eastern side of the shoal complex (Figure 5). The coarsest sands were associated with the central axis of the shoals. Mud fractions were typically <20%, but ranged up to 55% in a few samples and were dominated by very fine silts. Gravel patches contained shell hash and were found inshore of the 10-m isobath.

4.2 Annual-scale sediment-transport pathways and forcing mechanisms

During the November 2019 to September 2020 mooring deployment at S1A (31-m depth), ice cover was present from mid-December to early May (Figure 6). Winds were variable but typically less than 10 m/s (Figure 6A). Water depths varied between $\sim$30 and 32 m (Figure 6C), which primarily reflected wind dynamics (this area is microtidal). Currents at 3 meters above the bed were weakest during the ice-covered winter period, and strongest in November and December during the freezeup season. Current speeds were typically less than 0.3-0.5 m/s, except during brief events (Figure 6E). Current directions alternated between northeast and southwest (Figure 6C) and typically responded to changes in wind patterns (Figure 6B, D, F). Wave heights gradually increased throughout the open-water season from ∼0.5-1 m in the summer to ∼2-3 m in the fall (Figure 6G).

The long-term average current-driven bed stress (τ_c) was 0.075 N/m^2, less than the critical bed stress of 0.19 N/m^2 (Figure 6I). A few peaks in τ_c occurred throughout the deployment, leading to 786 hours of critical stress exceedance or "excess stress" by currents alone. This was equivalent to ∼10% of the November 2019 to September 2020 deployment period. The average wave-driven bed stress (τ_w) was 0.15 N/m^2. Multiple peaks in wave stress occurred, and the maximum value was 3.6 N/m^2. Wave stress exceeded the critical stress for 631 hours, or ∼8% of the deployment period. Waves contributed to excess stress primarily during September and November. Currents provided excess stress episodically throughout the entire deployment, including periods of ice cover (Figure 6K).

Near-bed suspended sediments (measured at 3 m above the bed) generally traveled parallel to the regional coastline (northeastward or southwestward; Figure 7A, C). During the fall storm season, transport was dominantly southwestward. During the winter-ice covered period, transport was dominantly northeastward. During the lower-energy summer open-water season, transport directions were variable over time scales corresponding to variations in wind patterns (figures 6C, 7A,). In surface waters, suspended-sediment transport was weaker and generally directed toward shore, except during fall freezeup and early winter when transport was directed dominantly along-coast (Figure 7).

4.3 Event-scale hydrodynamics and sediment transport

During the November 2019 wave event, CTDTu and LISST profiles were collected at the sites shown in Figure 8A at the same time that the mooring was deployed at S1A. Mooring time-series data from the event period are illustrated in Figure 8B-D, and size, turbidity, and temperature profiles from discrete locations in Figure 8A are presented in a stacked time-series view in Figure 8E-G. During the event, winds blew from the northeast for several days with variable speeds less than 5 m/s (Figures 6B, 8B). Toward the end of the event (Nov 23) onshore winds developed. Near-bed currents were generally southwestward (Figure 8C). Wave heights were generally >2 m with a peak on Nov 21 (Figures 6H, 8C). Wave-induced shear stresses exceeded the critical stress at that site for several days. In the water column, suspended-particle sizes were ∼100 μm during the peak in wave energy, but decreased throughout the rest of the period to <50 μm (Figure 8E). Turbidities were generally higher in shallower waters (up to ∼40 NTU) and near the bed at deeper sites (>40 NTU; Figure 8F). Warm water was mixed throughout the water column at some times early in the event, but by November 23 the inshore waters had cooled and offshore waters had re-stratified (Figure 8G). Water-column turbidities returned to near-background levels and suspended particle sizes decreased within a day of the change in wind and current direction and re-establishment of stratification.

4.4 Multidecadal trends in sediment transport potential

Based on the ERA5 trend analysis, the open-water season at Icy Cape has increased at a rate of ∼1.3 d/yr, similar to trends reported for the region by others (Farquharson et al., 2018; Figure 9A). It is worth noting that there was an apparent increase in the overall rate of change around 1990.

Also based on ERA5, the annual mean peak wave period increased at a rate of 0.019 s/yr (Figure 9B) and the annual mean significant wave height increased at a rate of 0.0050 m/yr (Figure 9C). These amount to increases of approximately 1 s in annual mean peak wave period and 0.35 m in significant wave height over the ∼70-year hindcast period. The annual mean shear stress, which ranged from ∼0.12 to 0.36 cm/s, also showed a slight increasing trend (Figure 9D).

The total hours of excess stress (or critical stress exceedance) generated by waves for sands increased at a rate of ∼2.6 hours per year (∼7.6 days in 70 years; Figure 9E). Similar to the number of open-water days per year, this parameter appeared to increase more rapidly beginning in the 1990s. The mean value between 1953 and 1989 was 34 hrs per year, and the mean value between 1990 and 2022 was 148 hours per year - representing a roughly five-fold increase, but still a small fraction of the year (148 hours is 1.7% of the year). Based on a comparison of bed stress during the three years at the beginning of the record (1953-1955) versus the end of the record (2020-2022), the annual "stress climate" changed from a few brief storm peaks occurring during September/October to a prolonged period of storm peaks between September and mid-December (Figure 9). Bed stress also occurred earlier in the year at the end of the record, but values remained below the critical stress threshold until mid-September (similar to the beginning of the record).

5 Discussion

Icy Cape and Blossom Shoals represent a sandy cape-shoal system similar in morphology to some analogous temperate systems, but influenced by sea ice. Ice causes physical disturbance (keel scours), blocks wave energy in the winter, and alters current flow in the winter by sheltering the water water column from wind forces. The future evolution of Blossom Shoals under diminishing sea ice and increasing wave energy remains unknown. Here we summarize observed morphology and seasonal transport dynamics, and discuss the implications of the changing wave climate on sediment transport.

5.1 Morphology and sediment properties of Blossom Shoals and comparisons to two temperate shoals

The morphology of Blossom Shoals generally resembles that of other cape-associated shoals found in temperate latitudes. The largest sand ridges at Blossom Shoals are 3-15 m high with wavelengths of 400-3300 m and occur within ~2 km of shore. By comparison, Diamond Shoals offshore of Cape Hatteras are up to 10 m high, spaced up to 5000 m apart, and occur within 10 km of shore (Hunt et al., 1977). Cape Lookout Shoals are ~2-7 m high, spaced up to 2000 m apart, and occur within 16 km of shore (McNinch & Wells, 1999). All three of these example systems have formed inshore of the 30-m isobath in relatively low-relief microtidal shelf settings.

In Blossom Shoals, most sediments are very fine to coarse sand (0 to 4ϕ) with a relatively high degree of sorting (Figure 5), and the dominant size is fine sand ($\sim 2.3\phi$). Muds and gravels are found infrequently in troughs between sand ridges, and muds are most common northeast of the cape (Figure 5). Finding well-sorted sands is expected in this type of environment. Mud is relatively scarce - a few small rivers feed the Alaskan Chukchi margin, and as Phillips and Reiss (1984) suggest, the majority of the local fine-grained fluvial sediment load (silts and clays carried in suspension) is likely trapped in the adjacent lagoons (similar to the trapping that occurs in the lagoons backing the North Carolina capes). Fall storms, such as those observed in November 2019, likely generate waves and remobilization of some of this stored mud, which is then available to be advected through the inlets by currents (see also Phillips & Reiss, 1984). Outside of the lagoons, fine-grained sediment is transported past the shoals in low concentrations, but has little opportunity to deposit and accumulate except in a few sheltered areas between ridges during low-energy seasons. The several days of sustained excess wave stress during the November 2019 event highlight one of the barriers to deposition (Figures 6J, 8D).

The sands comprising Blossom Shoals are somewhat finer than the dominantly 0-2 ϕ sand found at Diamond Shoals in North Carolina (Hunt et al., 1977). The finer sizes in Blossom Shoals may reflect regional lithology of the source material, and/or possibly the reduced energy climate associated with up to 9 months of ice cover per year and limited fetch during the summer season.

In Blossom Shoals and the two North Carolina systems, small sand waves are superimposed on top of the sand ridges, and are interpreted as evidence of active bedload transport (Phillips & Reiss, 1984; Hunt et al., 1977; Thieler et al., 2014). In the case of Blossom Shoals, Phillips and Reiss (1984) noted that migration of these sand waves is also responsible for filling keel scours which form during the winter - a process which was observed in successive years in this study (Figure 4). Ice gouging thus does not seem to be a major agent of morphologic change, though it does cause local and temporary disturbance.

Because there are so many morphologic similarities between Blossom Shoals and some North Carolina systems, it is interesting that the two temperate systems extend farther from shore than the arctic system (10-16 km in North Carolina, versus 2 km for Blossom Shoals). This raises the question of whether Blossom Shoals is limited in extent because there is too little sediment in the longshore transport cells to feed it, and/or because convergent offshore transport is too limited by the brief open-water season (and/or weak wave climate) to promote more extensive seaward shoal growth. In either case, a longer open-water season combined with a related intensification in wave climate could promote stronger longshore transport (which would accelerate sediment delivery to the headland) and consequently stronger offshore transport through convergence of longshore sediment flux from east and west. Transport patterns would also depend, of course, on sediment supplies and on the nature of the convergent currents, mediated by winds, waves, and the Alaska Coastal Current.

Over the past 70 years, the morphology of Blossom Shoals has been relatively stable in profile view (Figure 2). The large, concentric sand ridges appear to have migrated little, if at all, since the 1950s NOAA surveys (Figure 2), and the smaller bedforms found on the sides of the large sand ridges are remarkably similar in terms of locations and geometry to those described by Phillips and Reiss (1984). It thus appears that the shoal system has existed in a state of dynamic equilibrium not yet perturbed by changes in wave climate and a lengthening open-water season. An exception may be the small sand ridges most proximal to the headland, which appear to have migrated slightly seaward on the order of 100 m laterally - but due to the sparse data interpolated from the older survey charts, these changes should not be over-interpreted. These inner shoals may also behave somewhat differently than the outer shoals because of the dynamics of landfast ice. In the Arctic, landfast ice tends to form earlier in the fall than offshore ice, and break up later in the spring - and at this site, landfast ice tends to form inshore of site S1A (see Hošeková et al., 2020 and Hošeková et al., 2021 for discussions of landfast ice at this site).

5.2 Suspended-sediment transport dynamics

While fine-grained sediments (silts and clays) are found only in sheltered patches within the shoals, their transport during an annual cycle lends insight into general sediment pathways and potential bypassing around the shoals (with potential implications for nutrient transport and substrate character).

During the winter after ice forms, a weak signal of fine-grained suspended-sediment transport is observed near-bed with a persistent northeastward direction (Figure 7A). This wintertime suspended sediment follows the pathway of the Alaska Coastal current. During the open-water season, episodic wind events like those illustrated in Figure 6 (right column) and Figure 8 (first part of time series) disrupt this current flow. During these types of events, waves drive resuspension and elevated water-column turbidities, particularly in shallow nearshore zones (where mud tends to be more available; Figures 5, 8F). Wind-driven currents mix the water column (Figure 8E, F, G), disrupt the northeastward flow of the Alaska Coastal Current (Figure 8B, C), and drive brief southwestward transport of suspended sediments near bed (and landward transport of sediments near the surface; Figure 7). Annually, however, the net transport direction appears to be northeastward, meaning there should be a net transfer of particles toward the Arctic Ocean (and perhaps Barrow Canyon farther north). Given a longer open-water season, this net northeastward transport may weaken. This could have several implications include reduced northeastward transport of any sediment-associated nutrients and longer residence time of fine-grained sediments within the Chukchi Sea.

5.3 Measured and projected bed stresses

Seabed stresses imposed by waves and currents (and combined wave-current effects) are commonly used in sediment transport-rate equations. It is thus useful to evaluate seasonal variability in bed stresses to determine when the sands comprising the shoals are most likely to be mobile (i.e., times of excess stress, as noted in section 5.2), as well as interannual variability in mobility, in order to better predict whether sand transport potential has changed over the past few decades and determine the direction of present trends.

Between the early 1950s and mid-1990s, the mean number of open-water days per year was typically 50-150 at site S1A (which is outside the modern seasonal landfast ice zone observed by Hošeková et al., 2021). Excess stress generated by waves occurred for a much smaller portion of the year (<100 hrs per year; Figure 9A, E). This excess stress typically only occurred toward the end of the open-water season, in September. In the mid-1990s, the length of the open-water season began increasing to typical values closer to 200 days per year. This change was logically accompanied by an intensification of the wave climate (see Figure 9B, C), which has been attributed to increasing fetch as a consequence of increasing seasonal retreat of pack ice in the Arctic Ocean (Thomson & Rogers, 2014; Khon et al., 2014; X. L. Wang et al., 2015; Thomson et al., 2016; Liu et al., 2016; Casas-Prat et al., 2018). The increasing number of open-water days and more energetic sea states have jointly created a longer season of more frequent critical stress exceedence (Figure 9F). Interestingly, this period of high bed stress doesn't appear to start earlier than it did in the 1950s, which is likely a consequence of the onset of the fall storm season set by processes in the northern Pacific. But this high-stress period does extend much later into the year - i.e., into mid-December rather than mid-October. Consequently, the number of hours of sand mobility per year have increased.

It is worth noting that these changes may be conservative estimates of how the stress distribution has changed for the shoals, because (1) they don't account for currents and (2) these data are from a relatively deep site (S1A, 31 m). The actual bed stress acting on the seafloor is a non-linear combination of wave and current stress. Currents are not represented in the multidecadal analysis (Figure 9) because of limitations in the hindcast data, and currents would serve to amplify the stress imposed by waves. In terms of water depth, S1A is likely below the wave base for many locally and distally generated waves. Multidecadal reductions in sea ice have allowed for larger, longer-period waves to develop, which should provide increasing bed stress at site S1A and on the outer shoals. The inner shoals are likely impacted in a different way. While these longer-period waves may attenuate before they reach the inner shoals, the longer open-water season means there is a longer period each year when smaller waves can impact the shoals - though the multidecadal trends in landfast ice (which buffer the inner shoals against wave energy) are not well-known.

The increasingly long exposure to excess stress (at least at the outer shoals) should create greater rates of bedload transport in the shoals. Thus far, the shoals do not appear to have migrated substantially in response to these changes, unless the morphologic differences within 3 km of shore can be interpreted as meaningful (Figure 2; see also section 4.1). However, at some point in the future they will likely reach a tipping point when the overall morphology may change. A morphodynamic model of shoal evolution would be helpful in predicting such changes. Challenges to modeling would include (1) assessing the source term of sediment, i.e., rates of longshore drift and sizes of material supplied from adjacent shorelines and (2) assessing how eddies shed by the Alaska Coastal Current around the headland may influence the net directions of sediment transport (given that the Alaska Coastal Current is not necessarily static in time).

6 Conclusions

Icy Cape and Blossom Shoals are a cape-shoal system located along the Chukchi Sea coast in northwestern Alaska which represent a site of convergent sediment transport similar in nature to analogous temperate systems, such as the the multiple cuspate headlands forming the Outer Banks in North Carolina. Blossom Shoals consists of large sand ridges with relief of several meters and spacing of hundreds of meters. Patches of sand waves with relief on the order of a meter and spacing of tens of meters occur on the flanks of the larger ridges in many locations, and indicate active several transport (as evidenced by the “healing” of ice keel scours between seasons).

Unlike temperate systems, much of the wave-enhanced sediment transport that occurs is limited to the brief open-water season (though currents do act throughout the year - including during the winter - to occasionally mobilize seabed sands). The influence of waves is increasing due to increasingly energetic sea states and increasingly long periods of open water, which are both a consequence of diminishing Arctic pack ice. Based on modeled wave hindcasts for the past $\sim$70 years, the typical number of hours of excess stress generated by waves (at a $\sim$30-m site) has increased from $<$ 100 hours per year to $\sim$100-200 hours per year. Recent measurements suggest that annual hours of stress exceedence may be much higher. To date the shoals have exhibited little morphologic change, but a morphodynamic model which accounts for changes in seastate would be a worthwhile next step to assess whether a tipping point in morphology evolution may occur given further increases in wave exposure. The role and future fate of landfast ice, which historically occurs within 10 km of the shore, should also be considered since it may dramatically affect the total wave exposure in the inshore portion of the shoal (Hošeková et al., 2021).

Fine-grained sediments are sparse, but their transport is regulated by wind events and winter ice conditions. During the winter, suspended sediment travels in a net northeastward direction, toward the Arctic Basin. During wind events in the open-water season, this direction is reversed - though the net transport direction is still dominated by winter conditions. If the length of the open-water season maintains its present trajectory, there is a potential for the net transport direction to change, which could have implications for residence time of fine-grained sediment in the Chukchi Sea and nutrient pathways.

Acknowledgments

This work was funded by NSF OPP 1913195 and OPP 1818485. We thank the captains and crew of *R/V Sikuliaq* and Alex de Klerk for assistance in data collection, and

Steve Roberts for assistance with 1950s bathymetry acquisition and gridding, as well as McKenzie McLean, Owen White, and Tyler Souza for assistance with sample processing and discussions of results.

The S1A mooring data are available at http://hdl.handle.net/1773/47139 or

https://doi.org/10.18739/A2DF6K45W. The grain-size and water-column profile data are available at the Arctic Data Center under doi:10.18739/A2862BD1G (Eidam et al., 2023).

References

Aagaard, K., Weingartner, T. J., Danielson, S. L., Woodgate, R. A., Johnson, G. C., & Whitledge, T. E. (2006). Some controls on flow and salinity in Bering Strait. *Geophysical Research Letters*, *33*(19).

Ashton, A., Murray, A. B., & Arnoult, O. (2001). Formation of coastline features by large-scale instabilities induced by high-angle waves. *Nature*, *414*(6861), 296–300.

Barnes, P. W., Reimnitz, E., Hunter, R. E., Phillips, R. L., & Wolf, S. (1983). Geologic processes and hazards of the Beaufort and Chukchi Sea shelf and coastal regions. *OCSEAP Final Report, Research Unit*, *205*, 1–18.

Casas-Prat, M., Wang, X. L., & Swart, N. (2018). CMIP5-based global wave climate projections including the entire arctic ocean. *Ocean Modelling*, *123*, 66–85.

Creager, J. S., & McManus, D. A. (1968). *Geology of the floor of Bering and Chukchi Seas: American studies.* University of Washington Department of Oceanography.

Dyer, K. R., & Huntley, D. A. (1999). The origin, classification and modelling of sand banks and ridges. *Continental Shelf Research*, *19*(10), 1285–1330.

Eidam, E., Thomson, J., Malito, J., & Hošeková, L. (2023). *Blossom Shoals water-column, seabed sediment, and bathymetry data. Icy Cape, Chukchi Sea, Alaska. 2019-2020.* Arctic Data Center. Retrieved from `https://arcticdata.io/catalog/view/doi:10.18739/A2862BD1G`

Fang, Y., Potter, R. A., Statscewich, H., Weingartner, T. J., Winsor, P., & Irving, B. K. (2017, December). Surface Current Patterns in the Northeastern Chukchi Sea and Their Response to Wind Forcing. *Journal of Geophysical Research: Oceans*, *122*(12), 9530–9547. Retrieved 2021-01-26, from https://onlinelibrary.wiley.com/doi/abs/10.1002/2017JC013121 doi: 10.1002/2017JC013121

Farquharson, L. M., Mann, D., Swanson, D., Jones, B., Buzard, R., & Jordan, J. (2018). Temporal and spatial variability in coastline response to declining sea-ice in northwest Alaska. *Marine Geology*, *404*, 71–83.

Gibbs, A. E., Nolan, M., Richmond, B. M., Snyder, A. G., & Erikson, L. H. (2019). Assessing patterns of annual change to permafrost bluffs along the North Slope coast of Alaska using high-resolution imagery and elevation models. *Geomorphology*, *336*, 152–164.

Gibbs, A. E., & Richmond, B. M. (2015). *National assessment of shoreline change: historical shoreline change along the north coast of Alaska, US-Canadian border to Icy Cape.* US Department of the Interior, US Geological Survey Reston, VA, USA.

Grant, W. D., & Madsen, O. S. (1979). Combined wave and current interaction with a rough bottom. *Journal of Geophysical Research: Oceans*, *84*(C4), 1797–1808.

Grantz, A., Dinter, D. A., Hill, E., May, S., McMullin, R., Phillips, R., & Reimnitz, E. (1982). *Geologic framework, hydrocarbon potential, and environmental conditions for exploration and development of proposed oil and gas lease sale 87 in the Beaufort and northeast Chukchi Seas: A summary report* (Tech. Rep.). US Geological Survey.

Hošeková, L., Eidam, E., Panteleev, G., Rainville, L., Rogers, W. E., & Thomson, J. (2021). Landfast ice and coastal wave exposure in northern Alaska. *Geophysical Research Letters*, *48*(22), e2021GL095103.

Hošeková, L., Malila, M. P., Rogers, W. E., Roach, L. A., Eidam, E., Rainville, L., … Thomson, J. (2020). Attenuation of ocean surface waves in pancake and frazil sea ice along the coast of the Chukchi Sea. *Journal of Geophysical Research: Oceans*, *125*(12), e2020JC016746.

Hunt, R. E., Swift, D. J., & Palmer, H. (1977). Constructional shelf topography, Diamond Shoals, North Carolina. *Geological Society of America Bulletin*, *88*(2), 299–311.

Jones, B. M., Arp, C. D., Jorgenson, M. T., Hinkel, K. M., Schmutz, J. A., & Flint, P. L. (2009). Increase in the rate and uniformity of coastline erosion in Arctic Alaska. *Geophysical Research Letters*, *36*(3), n/a–n/a. Retrieved from `http://dx.doi.org/10.1029/2008GL036205` (L03503) doi: 10.1029/2008GL036205

Khon, V., Mokhov, I., Pogarskiy, F., Babanin, A., Dethloff, K., Rinke, A., & Matthes, H. (2014). Wave heights in the 21st century Arctic Ocean simulated with a regional climate model. *Geophysical Research Letters*, *41*(8), 2956–2961.

Komar, P. (1976). *Beach processes and sedimentation.* Prentice-Hall, Inc., New Jersey.

Liu, Q., Babanin, A. V., Zieger, S., Young, I. R., & Guan, C. (2016). Wind and wave climate in the Arctic Ocean as observed by altimeters. *Journal of Climate*, *29*(22), 7957–7975.

Madsen, O. S. (1994). Spectral wave-current bottom boundary layer flows. In *Coastal Engineering 1994* (pp. 384–398).

Mahoney, A. R., Eicken, H., Gaylord, A. G., & Gens, R. (2014). Landfast sea ice extent in the Chukchi and Beaufort Seas: The annual cycle and decadal variability. *Cold Regions Science and Technology*, *103*, 41–56.

McCarroll, R. J., Masselink, G., Valiente, N. G., Wiggins, M., Scott, T., Conley, D. C., & King, E. V. (2020, April). Impact of a headland-associated sandbank on shoreline dynamics. *Geomorphology*, *355*, 107065. Retrieved 2021-01-26, from `https://linkinghub.elsevier.com/retrieve/pii/S0169555X20300374` doi: 10.1016/j.geomorph.2020.107065

McNinch, J. E., & Luettich, R. A. (2000). Physical processes around a cuspate foreland: implications to the evolution and long-term maintenance of a cape-associated shoal. *Continental Shelf Research*, 23.

McNinch, J. E., & Wells, J. T. (1999, June). Sedimentary processes and depositional history of a cape-associated shoal, Cape Lookout, North Carolina. *Marine Geology*, *158*(1-4), 233–252. Retrieved 2021-01-26, from `https://linkinghub.elsevier.com/retrieve/pii/S0025322798001698` doi: 10.1016/S0025-3227(98)00169-8

Moslow, T. F., & Heron, S. D. J. (1981). Holocene depositional history of a microtidal cuspate foreland cape: Cape Lookout, North Carolina. *Marine Geology*, *41*(3-4), 251–270.

Park, J.-Y., & Wells, J. T. (2005). Longshore transport at Cape Lookout, North Carolina: shoal evolution and the regional sediment budget. *Journal of coastal re-*

search, *21*(1), 1–17.

Phillips, R., Barnes, P., Hunter, R., Reiss, T., & Rearic, D. (1988). *Geologic investigations in the Chukchi Sea, 1984, NOAA ship SURVEYOR cruise* (Tech. Rep.). US Geological Survey,.

Phillips, R., & Reiss, T. (1984). *Nearshore marine geologic investigations, Icy Cape to Wainwright, northeast Chukchi Sea.* US Department of the Interior, Geological Survey.

Pickens, B. A., Taylor, J. C., Finkbeiner, M., Hansen, D., & Turner, L. (2021). Modeling sand shoals on the US Atlantic shelf: Moving beyond a site-by-site approach. *Journal of Coastal Research*, *37*(2), 227–237.

Short, A. D. (1975, March). Offshore Bars along the Alaskan Arctic Coast. *The Journal of Geology*, *83*(2), 209–221. Retrieved 2021-01-26, from `https://www.journals.uchicago.edu/doi/10.1086/628082` doi: 10.1086/628082

Short, A.-D. (1979). Barrier island development along the Alaskan-Yukon coastal plains. *Geological Society of America Bulletin*, *90*(1_Part_II), 77–103.

Showstack, R. (2013). Diminishing Sea Ice in the Arctic Presents Challenges and Opportunities. *Eos Trans. AGU*, *94*(31), 270–271. doi: 10.1002/2013EO310002

Soulsby, R. (1987). Calculating bottom orbital velocity beneath waves. *Coastal Engineering*, *11*(4), 371–380.

Soulsby, R. (1997). *Dynamics of marine sands.* Howbery Park, London, 142 pp.: HR Wallingford.

Soulsby, R., & Whitehouse, R. (1997). Threshold of sediment motion in coastal environments. *Pacific Coasts and Ports' 97: Proceedings of the 13th Australasian Coastal and Ocean Engineering Conference and the 6th Australasian Port and Harbour Conference; Volume 1*, 145–150.

Stabeno, P., Kachel, N., Ladd, C., & Woodgate, R. (2018). Flow patterns in the eastern Chukchi Sea: 2010–2015. *Journal of Geophysical Research: Oceans*, *123*(2), 1177–1195.

Stroeve, J., & Notz, D. (2018, sep). Changing state of Arctic sea ice across all seasons. *Environmental Research Letters*, *13*(10), 103001. Retrieved from `https://doi.org/10.1088%2F1748-9326%2Faade56` doi: 10.1088/1748-9326/aade56

Tanner, W., Evans, R., & Holmes, C. (1963). Low-energy coast near cape romano, florida. *Journal of Sedimentary Research*, *33*(3), 713–722.

Thieler, E. R., Foster, D. S., Himmelstoss, E. A., & Mallinson, D. J. (2014). Geologic framework of the northern North Carolina, USA inner continental shelf and its influence on coastal evolution. *Marine Geology*, *348*, 113–130.

Thomson, J., Eidam, E., & Hošeková, L. (2021). *Mooring results from Coastal Ocean Dynamics in the Arctic (CODA).* University of Washington. Retrieved from https://digital.lib.washington.edu/researchworks/handle/1773/47139

Thomson, J., Fan, Y., Stammerjohn, S., Stopa, J., Rogers, W. E., Girard-Ardhuin, F., ... others (2016). Emerging trends in the sea state of the Beaufort and Chukchi seas. *Ocean Modelling*, *105*, 1–12.

Thomson, J., & Rogers, W. E. (2014). Swell and sea in the emerging Arctic Ocean. *Geophysical Research Letters*, *41*(9), 3136–3140.

UAF. (2019). *Rolling Deck to Repository, Sikuliaq* (Tech. Rep. No. SKQ201923S). University of Alaska Fairbanks. (DOI : 10.7284/908599 (accessed December 21, 2022).)

Wang, Q., Zhang, M., Zhong, S., Du, G., Jin, B., Yang, H., & Song, C. (2009, September). Dynamic sedimentation and geomorphologic evolution of the Laizhou shoal, Bohai sea, Northern China. *Journal of Asian Earth Sciences*, *36*(2-3), 196–208. Retrieved 2021-01-26, from https://linkinghub.elsevier.com/retrieve/pii/S1367912009001333 doi: 10.1016/j.jseaes.2009.06.001

Wang, X. L., Feng, Y., Swail, V. R., & Cox, A. (2015). Historical changes in the beaufort-chukchi-bering seas surface winds and waves, 1971-2013. *Journal of Climate*, *28*(19), 7457–7469.

Wiberg, P. L., & Sherwood, C. R. (2008). Calculating wave-generated bottom orbital velocities from surface-wave parameters. *Computers & Geosciences*, *34*(10), 1243–1262.

Woodgate, R. A., & Aagaard, K. (2005). Revising the Bering Strait freshwater flux into the Arctic Ocean. *Geophysical Research Letters*, *32*(2).

Woodgate, R. A., Stafford, K. M., & Prahl, F. G. (2015). A synthesis of year-round interdisciplinary mooring measurements in the Bering Strait (1990–2014) and the RUSALCA years (2004–2011). *Oceanography*, *28*(3), 46–67.

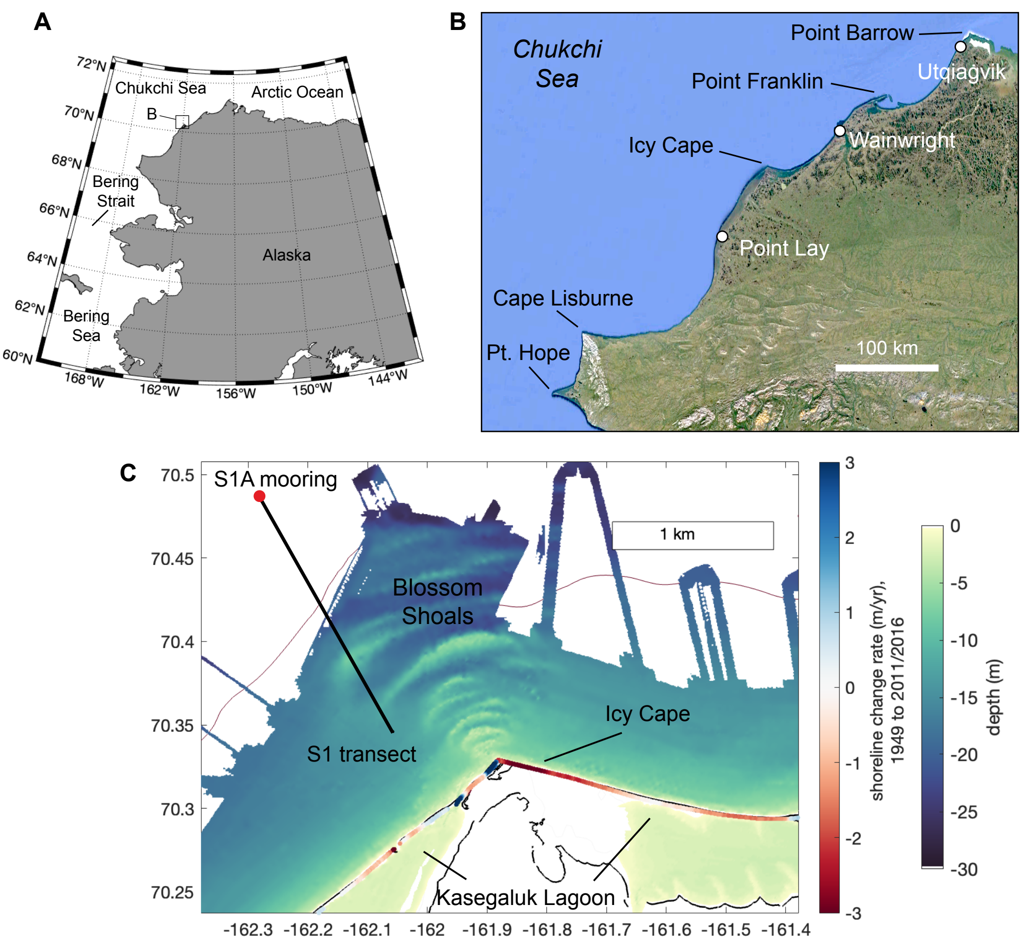

Figure 1: Vicinity maps. A) Icy Cape is located in northwestern Alaska on the Chukchi Sea. B) Cuspate headlands of northwestern Alaska, including Icy Cape. C) Blossom Shoals extend seaward a few kilometers from Icy Cape. Sources of bathymetry and shoreline change data provided in text.

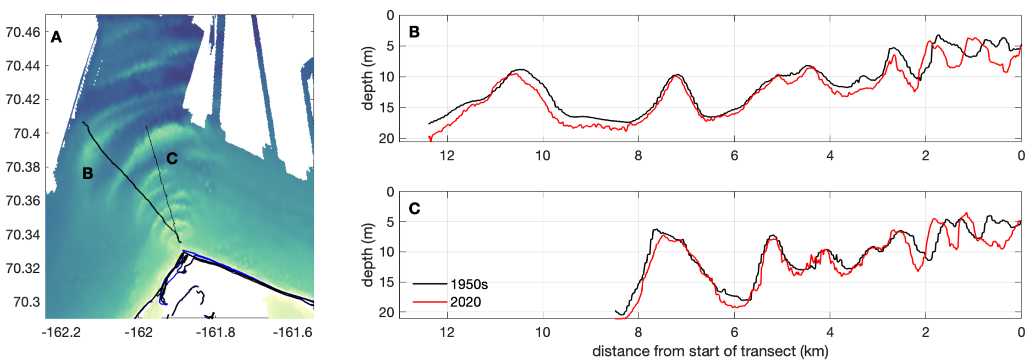

Figure 2: Shoal bathymetry. a) Gridded 1950s bathymetry of Blossom Shoals. b) Southern elevation profile of the shoals, from 1950 (based on gridded NOAA charts; see text) and 2020 (using a single-beam system on a small boat). c) Same as (b) for northern transect shown in (a). Vertical errors are not well-constrained and not shown. The general location of shoals which are >2 km from shore has remained relatively unchanged in 70 years (see discussion in text.

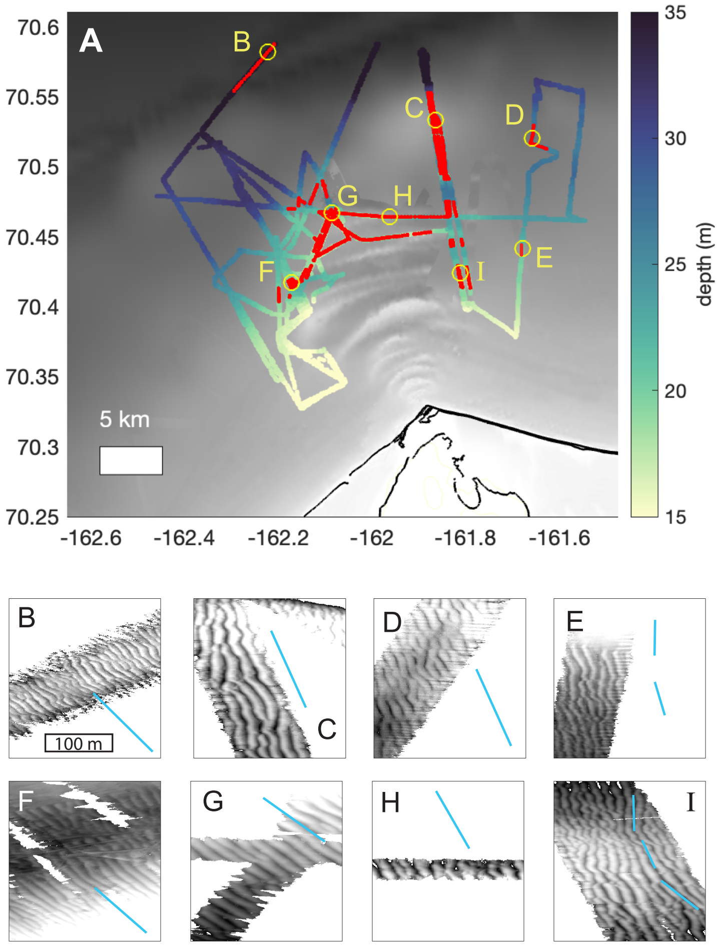

Figure 3: Bedform occurrence and details. A) Bedform occurrence (red) along 2019 and 2020 survey tracks (shaded by depth). Yellow dots denote regions highlighted in subsequent panels. (B-F) Details of ripples. Scale in each panel is the same. Blue lines denote general orientation of bedform crests. Bedform heights were typically 1 m and wavelengths were on the order of 10-20 m.

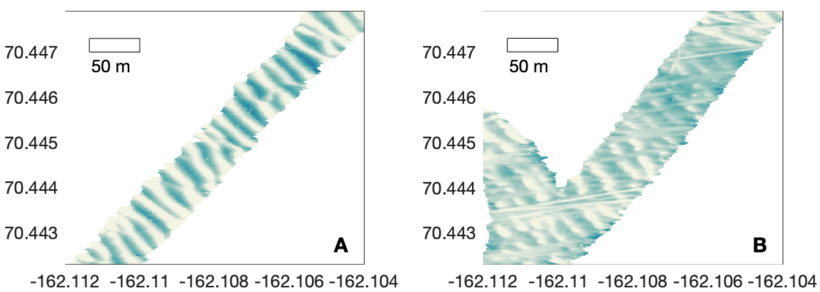

Figure 4: Detail of the change in bedforms between (A) November 2019 and (B) October 2020 at the same location (near site G in Figure 3. Note the linear scarring in (B); these data were collected earlier in the season than those in panel (A)

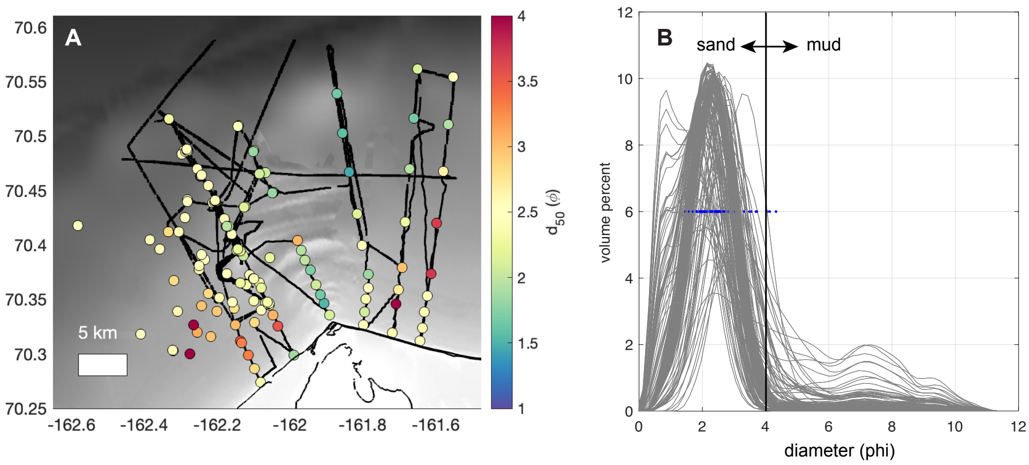

Figure 5: Seabed grain sizes. A) Map of median sediment diameter (d_{50}) reported on the phi scale (the $\log_2$ of the diameter in millimeters). Ship survey tracks are shown in black. Sediments were generally sandy except for a few regions near shore where muds were dominant. B) Aggregated histograms (by volume percent) for sample sites shown in (A). Blue dots denote d_{50} values. Histograms are shown to provide context regarding sorting (i.e., the width of the grain-size distribution peaks). Sand sizes from 1 to 3 phi were common (coarse to fine sand). Note that bimodal samples represent mud-dominated sites. FIX HISTOGRAM TO INCLUDE 2020 DATA

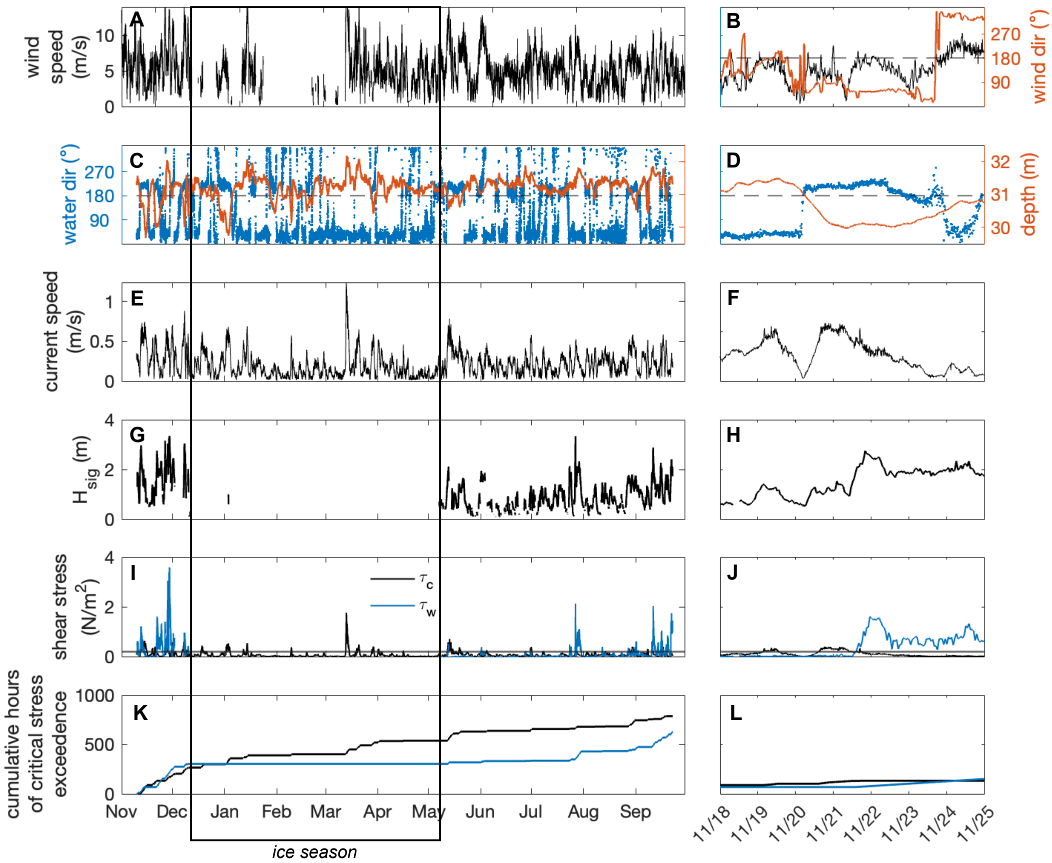

Figure 6: Meteorological data (from Wainwright) and mooring data (from S1A) for 2019 to 2020. The panels at left span the entire mooring record and the panels at right show a magnified view of mid-November 2019, when high-density vessel-based sampling was conducted. A, B) Wind speed. C, D) Water direction and depth. E, F) Current speed averaged between 3 and 21 meters above the bed. G, H) Significant wave height. I, J) Current and wave shear stress (with critical stress shown by the horizontal line). K, L) Cumulative hours when the critical stress was exceeded by waves or currents.

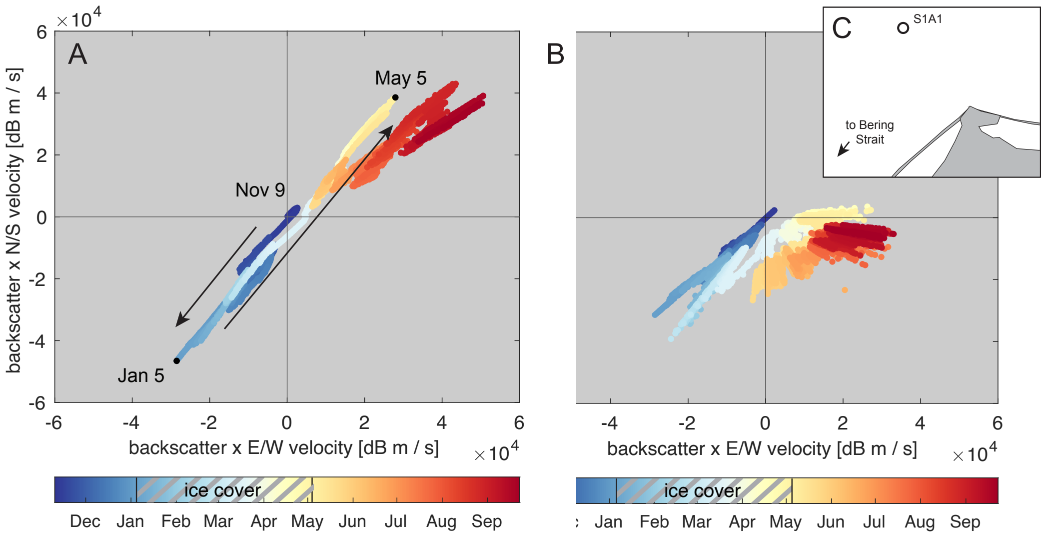

Figure 7: Cumulative sediment flux (proxy measure, using ADCP backscatter multiplied by velocity) in earth coordinates for the mooring deployment period, at site S1A. A) Flux at 3 meters above the bed. Arrows denote major net transport directions in fall (left) and winter (right). Ice cover was present from early January to May 5. Jan 5 and May 5 denote the transition points when the general flux direction abruptly changed. B) Flux at 21 meters above the bed (near the water surface). C) Schematic of local shoreline orientation for reference.

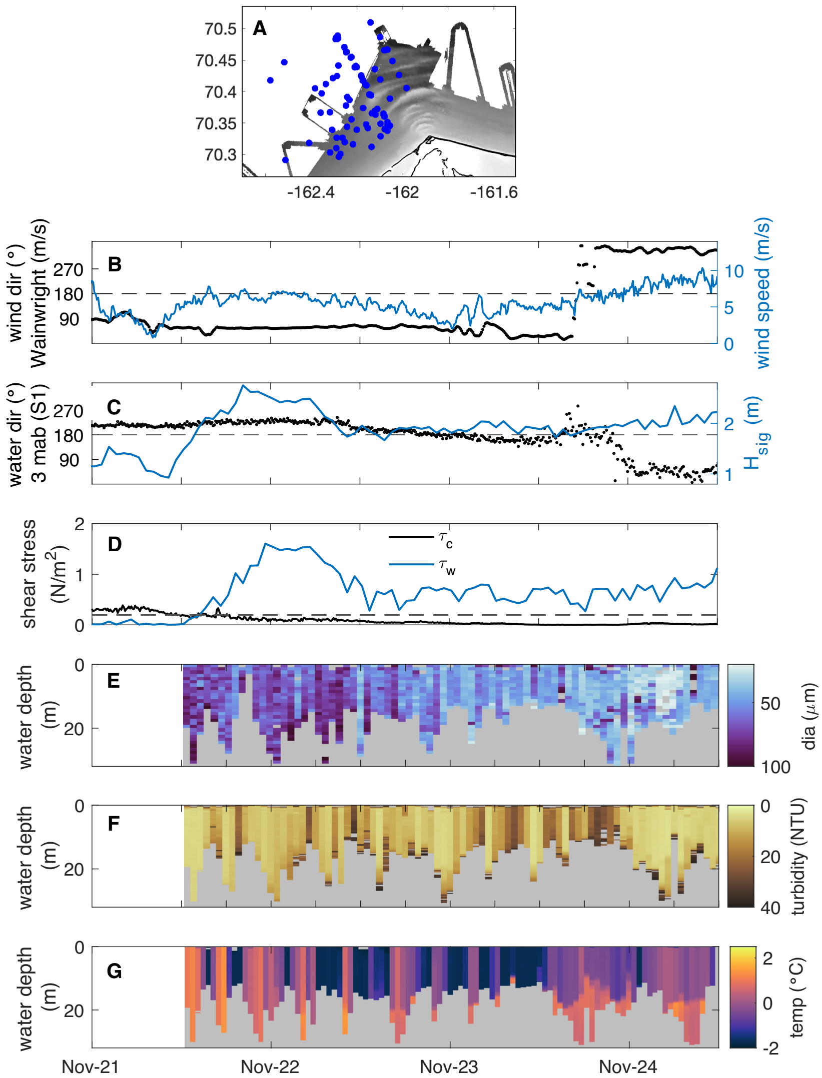

Figure 8: Hydrodynamics and water-column properties during the November 2019 wave event. A) Locations of CTDTu/LISST profiles. B) Wind direction and wind speed at Wainwright (see Figure 1B). C) Water direction and significant wave height at the S1A tripod (31 m water depth, 3 m above bed). D) Bed shear stress at S1A (current- and wave-induced). E) Water-column profiles of mean particle diameter throughout the study area. F) Water-column profiles of turbidity. G) Water-column profiles of temperature. Note that panels E-G are presented as time series though each profile was collected at a different location (the sites in A). They are shown in this fashion to give a general sense of the temporal evolution of suspended-sediment characteristics.

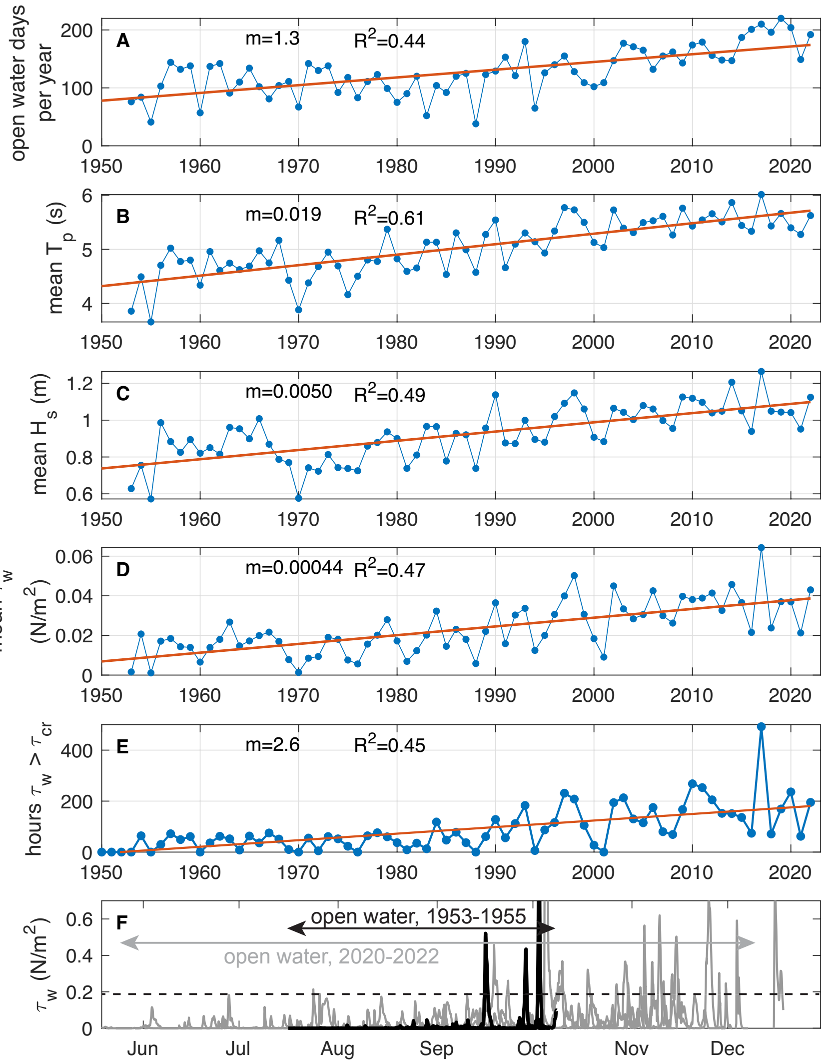

Figure 9: Multi-decadal trends in parameters related to waves and bed stresses, derived from ERA5 output. A) Number of open-water days per year. B) Mean peak wave period during each annual open-water season. C) Mean significant wave height during each annual open-water season. D) Mean τ_w during each annual open-water season (calculated from T_p and H_s). E) Cumulative number of hours per year when $\tau_w > \tau_{wcr}$ (0.196 N/m^2). F) Seasonal record of τ_w calculated from ERA5 output for the years 1954-1956 (black) and 2020-2022 (gray). The dashed line denotes τ_{wcr}.